UNIVERSITÀ
DEGLI STUDI
FIRENZE

DOTTORATO DI RICERCA IN
AREA DEL FARMACO E TRATTAMENTI INNOVATIVI

CICLO XXX

COORDINATORE Prof. Elisabetta Teodori

The pathophysiological role of the blood brain barrier in the oxaliplatin-induced neuropathy

Settore Scientifico Disciplinare BIO/14

Dottorando
Dott. Mario Maresca

Tutore
Prof. Carla Ghelardini

Coordinatore
Prof. Elisabetta Teodori

Anni 2014 /2017

Index

Abstract 4

1. Introduction 6

1.1 The blood brain barrier 7

1.1.1 Anatomy 7

1.1.2 Physiology and functions of BBB 8

1.2 The NeuroVascular Unit 9

1.2.1 Endothelial cells 10

1.2.1.1 Tight Junctions 11

1.2.1.2 Adherens junctions 13

1.2.2 Astrocytes 13

1.2.3 Pericytes 14

1.2.4 Extracellular Matrix 16

1.3 BBB under pathological conditions 17

1.3.1 BBB and neuropathic pain 17

1.4 Oxaliplatin - use and toxicity 18

1.4.1 Mechanism of action 20

1.4.2 Oxaliplatin-induced neuropathy 21

1.5 Oxaliplatin and BBB 24

1.6 Gap Junctions 25

1.6.1 Pannexin hemichannels 26

1.7 Pannexins and Connexins in the NeuroVascular Unit 27

1.7.1 Pannexin and connexins at the vascular wall 27

1.7.2 Pannexins and connexins in astrocytes and neurons 28

1.8 Pannexin and pain 29

2. Aim of the study 31

3. Materials and methods 34

3.1 Animals 35

3.2 In vivo oxaliplatin model 35

3.3 Ex vivo immunofluorescent staining 35

3.4 In vivo permeability 36

3.5 Cell line 37

3.6 MTT assay 37

3.7 Western blotting 38

3.8 In vitro immunofluorescent staining 38

3.9 Caspase-3 enzimatic activity 39

3.10 Extracellular ATP quantification 40

3.11 Calcium imaging 40

3.12 Statistical analysis 41

4. Results 42

4.1 Ex vivo analysis 43

4.2 In vivo permeability 44

4.3 MTT assay 45

4.4 ER stress - GRP78 expression 46

4.5 Ca^{2+} imaging - prolonged exposure to oxaliplatin 47

4.6 Caspase-3 activity and BAX expression 49

4.7 Cytochrome C release from mitochondria 52

4.8 ATP release - prolonged exposure to oxaliplatin 53

4.9 TJs and cytoskeleton distribution - prolonged exposure to oxaliplatin 54

4.10 Ca^{2+} imaging - acute effects of oxaliplatin 56

4.11 ATP release - acute effects of oxaliplatin 57

4.12 TJs and cytoskeleton distribution - short exposure to oxaliplatin 59

5. Discussion 60

6. Bibliography 69

Acknowledgments 91

Abstract

Oxaliplatin has become part of the world-wide standard of care for the adjuvant and the palliative treatment of the metastatic colon cancer. However, its efficacy is hampered by dose-limiting neurotoxicity, which leads to painful sensory neuropathy. Neurotoxicity can be manifested with two distinct syndromes: an acute one that onsets shortly after infusion, and a dose-limiting, cumulative sensory neuropathy. Paucity of information regarding the molecular basis of oxaliplatin-induced neuropathy makes difficult to find new therapeutic opportunities. Although alterations have been found in both peripheral and central nervous system, the latter is particularly distressed by antineoplastic treatment. Neurons and glial cells, in particular astrocytes, strongly react to oxaliplatin with a maladaptive response occurring in spinal and supra-spinal areas facilitating the chronicization of pain. To note, the relationship between neuropathic pain disorders and blood brain barrier (BBB) homeostasis alterations has been found. Interestingly, studies on non-human primates and rats revealed scarce capacity of the antineoplastic compound to cross the BBB after a single injection. The little amount found in the cerebrospinal fluid (CSF) could be enough to trigger acute pain sensitization as well as increased concentration could be reached after repeated administrations.

The aim of this study was to evaluate the interference of oxaliplatin with the BBB system in a rat model of oxaliplatin-induced neuropathy and in a rat brain endothelial cell line (RBE4). As first, the immunofluorescent staining detected IgG extravasation and reactive astrocytes in the lumbar blood spinal cord barrier (BSCB) of rats daily treated with oxaliplatin (2.4 mg kg^{-1}, *i.p*) for 14 days. Moreover, the *i.v.* injection of 10 kDa dextran texas red revealed enhanced permeability of the BBB/BSCB in specific brain and spinal cord areas crucially involved in the oxaliplatin-induced neuropathic pain sensitization (prefrontal cortex, somatosensory area S1 and lumbar spinal cord) after 7 days of chemotherapy treatment. Further, aimed to deeply explore the altered machinery of the endothelial compartment of the NVU, RBE4 cells were used to set up an *in vitro* model, which reproduced the vascular wall of the BBB. The vitality assay allowed choosing concentrations of oxaliplatin (10-30 μM) that slightly affected the RBE4 viability in 8-24 h period of

treatment, in order to mimic a damage that does not irreversibly alter the endothelial compartment of the NVU.

Results showed that sub-lethal concentrations were able to alter levels of GRP-78 (78 kDa glucose-regulated protein) as well as the cytoplasmic calcium concentration ($[Ca^{2+}]_i$), thus allowing the hypothesis of endoplasmic reticulum impairment. Furthermore, the sub-lethal concentrations of the antineoplastic agent activated caspase-3 after 8, 16 and 24 h treatment leaving unchanged expression of the pro-apoptotic factor Bax up to 16 h. Extracellular ATP concentration was also increased. Finally, the immunofluorescent staining revealed derangement of cytoskeleton protein F-actin and relocation of the tight junction protein ZO-1.

In conclusion, our data revealed the involvement of BBB's endothelial compartment in the pathophysiology of oxaliplatin-induced neuropathy.

1. Introduction

1.1 The blood brain barrier

1.1.1 Anatomy

All organisms with a developed Central Nervous System (CNS) have a blood brain barrier (BBB) (Abbott, 2005). The BBB is created by the endothelial cells that form the wall of the capillaries, both in the brain and in the spinal cord of mammals. The surface area of these microvessels constitutes the largest interface for blood-brain. Depending on the anatomical region, this surface area, is between 150 and 200 cm^2 g^{-1} tissue giving a total area for exchange in the brain of between 12 and 18 m^2 for the average human adult (Nag and Begley, 2005). Even the epithelial cells of the choroid plexus form an interface by facing the cerebrospinal fluid, so constituting the blood-cerebrospinal fluid barrier (BCSFB). The blood-spinal cord barrier (BSCB) has a similar cellular and molecular structure as the BBB; however, specific differences have been described. The BSCB for instance contains lower levels of occludin, ZO-1 and AJ proteins VE-cadherin and β-catenin. As a result, the barrier is more permeable to tracers and pro-inflammatory cytokines. Additionally, BSCB ECs express lower levels of P-glycoprotein, the major efflux pump in the BBB. Finally, Lower pericyte coverage was shown to correlate with the higher permeability of the BSCB in comparison to the BBB (Abbott et al., 2013).

Besides its barrier function, choroid plexus epithelial cells have a secretory function and produce the CSF. The barrier and secretory function of the choroid plexus epithelial cells are maintained by the expression of numerous transport systems allowing the directed transport of ions and nutrients into the CSF and the removal of toxic agents out of the CSF. The third interface is provided by the avascular arachnoid epithelium, underlying the dura, and completely enclosing the CNS; this completes the seal between the extracellular fluids of the central nervous system and that of the rest of the body (Abbott et al., 2006). However, since its avascular nature and relatively small surface area it does not represent a significant exchange surface area between the blood and the CNS (Kandel et al., 2000) (Fig. 1).

At all three interfaces, the barrier function results from a combination of physical barrier (tight junctions (TJs)) between cells reducing flux via the intercellular cleft or paracellular pathway, transport barrier (specific transport

mechanisms mediating solute flux), and metabolic barrier (enzymes metabolizing molecules in transit) (Abbott 2010).

The barrier function is not fixed, but can be modulated and regulated, both in physiology and in pathology (Abbott et al., 2006).

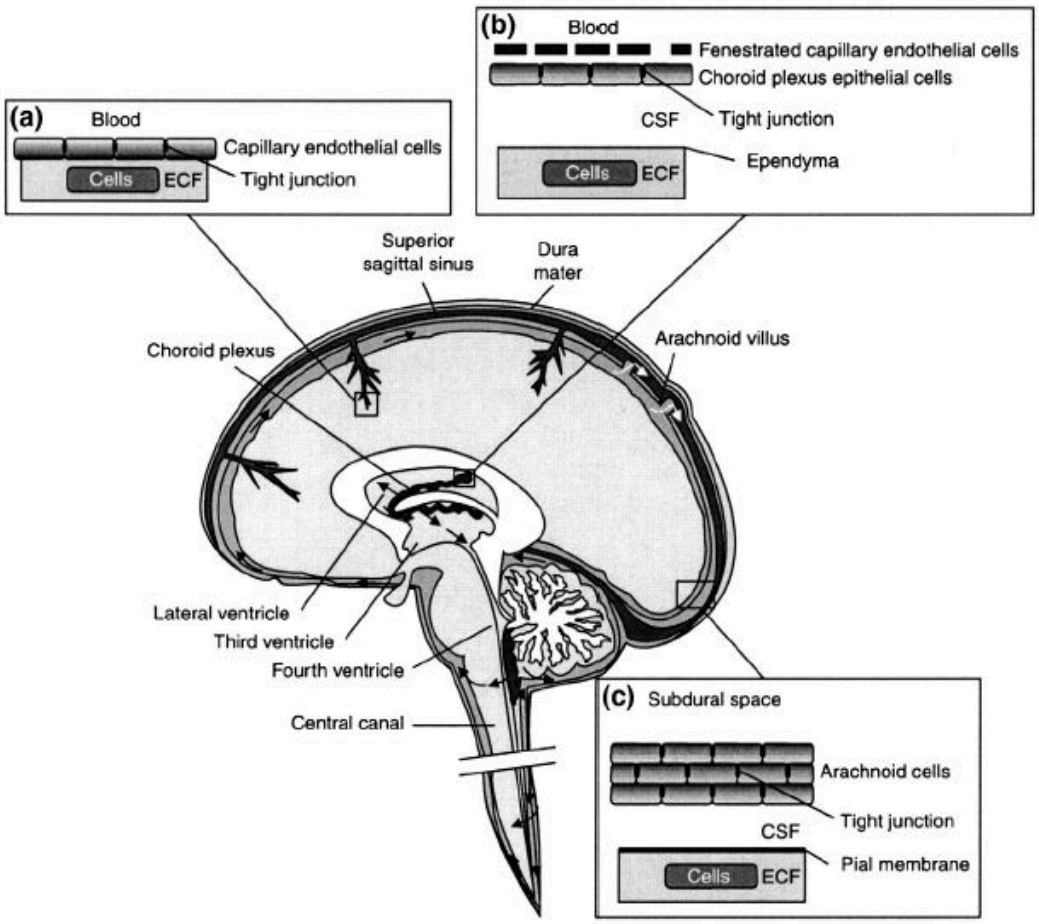

Figure 1. Barriers of the brain. The BBB proper barrier (**a**). The blood-CSF barrier (BCSFB) (**b**). The arachnoid barrier (**c**) (Abbott et al., 2010).

1.1.2 Physiology and functions of BBB

The barriers have dynamic functions and respond to signals from the blood and brain (Serlin et al., 2015) (see the table below).

The barriers are permeable gaseous molecules (O_2 and CO_2 N_2, Helium, Xenon) and several gaseous anaesthetics. Otherwise, lipids can pass by diffusion. Moreover, BBB is permeable to water but solute carriers on apical and basal membranes regulate the passage of small solutes. Multidrug transporter proteins control the concentration in the CNS of many molecules. They are ubiquitous transporters that, by the hydrolysis of ATP, can facilitate

the transport into the cell of some molecules and restrict the accumulation in the CNS of other molecules. Together with Pgp-like proteins, the multidrug transporters limit the access of drugs and other solutes (e.g. bilirubin, neurotoxins and the degradation product of haemoglobin) to the brain (Abbott and Friedman, 2012). Peptides and proteins exploit adsorptive- and receptor-mediated transcytosis mechanisms to cross the endothelial layer of the barriers. The insulin independent glucose transporter GLUT1 and the other isoforms (GLUT3 and GLUT4) actively transport sugars across the BBB, thus regulating the glucose uptake into the brain. Furthermore, endothelial cells (ECs) express other specific solute carriers to funnel amino acids across the lipid layers (Devaskar et al., 1991; Simpson et al., 2001). Ion channels and transporters of ECs keep the optimal ionic composition to allow the synaptic signalling function. Thanks to these transporters the potassium concentration of plasma (4.5 mM) is maintained different from K^+ in the CSF and the interstitial fluid (2.5 mM). In addition Ca^{2+}, Mg^{2+} and pH are actively regulated at BBB and BSCB levels (Abbott et al., 2010).

The barriers also regulate the recruitment and entry of leukocytes and innate immune elements and involve in both the reactive and surveillance functions of CNS immunity. Integrins and adhesion molecules such as ICAM-1 and PECAM-1, contribute to the adhesion and/or migration of distinct subsets of leukocytes to the CNS (Greenwood et al., 2003).

Table 1. (from Abbott, 2013).

Functions of the blood–brain barrier:
1. Controls molecular traffic, keeps out toxins (minimises neuronal cell death, preserves neural connectivity)
2. Contributes to ion homeostasis for optimal neural signalling
3. Maintains low protein environment in CNS, limits proliferation, preserves neural connectivity
4. Separates central and peripheral neurotransmitter pools, reduces cross-talk, allows non-synaptic signalling in CNS
5. Allows immune surveillance and response with minimal inflammation and cell damage

1.2 The NeuroVascular Unit

During the last decades, the concept of the BBB has evolved from one of a

mere endothelial barrier to a more integrative view in which the BBB is regarded a modulatory interface between the blood and the brain. The BBB, in this extended form, describes a number of processes that take place in the neurovascular unit (NVU). The first concept of NVU was defined by Harder (Harder et al., 2002) as a structure formed by mainly neurones, astrocytes, basal lamina covered with and pericytes, endothelial cells and extracellular matrix (Fig. 2). Each component is linked to each other, establishing an anatomical and functional whole, which results in a highly efficient system of regulation of cerebral blood flow (Armstead & Raghupathi 2011; Abbott & Friedman 2012). This interplay is allowed by gap junctions and adhesion molecules, such as cadherins and integrins (Simard et al., 2003; Del Zoppo 2010; Figley & Stroman, 2011). Gap junctions and ionic channels permit the passage of ions such as Ca^{2+} and K^{+}, as well as the action of neurotransmitters such as ATP (Gordon et al., 2007). Neurons and vascular cells, working together in concert thanks to their mieleu generate an integrated process, known as neurovsascular coupling, which allow brain and spinal cord homeostasis by providing the energy demands of neuronal activity via a tight, activity-dependent regulation on local blood flow (Serlin et al., 2015). Recent findings show that during BBB impairment, vessels improperly respond to neuronal impulse (Winkler et al., 2012). Under pathological conditions, the physiological neurovascular coupling may fail, and neuronal depolarization during seizures or spreading depolarization may be associated with no or "inverse coupling" (Serlin et al., 2015). The components of the NVU share the same embryonic origin and all of them are susceptible to both vascular endothelial growth factor (VEGF) and nerve growth factor (NGF) (Soker et al., 2002; Sanchez et al., 2013). Furthermore, each component seems to play specific roles in the regulation and the maintenance of the NVU homeostasis. However, the precise role of each constituent is still poorly understood (Kowianski et al. 2013).

1.2.1 Endothelial cells

ECs of the brain microvasculature have a characteristic phenotype that makes them different from ECs located elsewhere (Daneman, 2012). For example,

brain ECs, as well as epithelial cells, are polarized components throughout the expression of specific transporters and since they are connected by tight junctions that interfere with the paracellular transport of molecules and ions between cells (Nag, 2011; Daneman, 2012). Moreover, density of mitochondria in brain ECs is higher if compared with the peripheral vasculature, thus suggesting a major risk of reactive oxygen species (ROS) formation (Nag, 2011). By a structural point of view, ECs are in contact with astrocytic endfeet and pericyte through the basal lamina, forming, with neurons, the NVU (Hawkins and Davis, 2005; Stanimirovic and Friedman, 2012).

Functionally, ECs are important in the maintenance of BBB homeostasis thanks to the bidirectional transport across the brain through active efflux transport, protein and peptide carriers and ion transporters (Nag, 2011). Notably, a highly organized protein structure in ECs composed by adherent and tight junctions selectively restrict the passage of polar molecules such as amino acids, vitamins and nucleosides monocarboxylic acids (Grammas et al., 2011; Mokgokong et al., 2014). Importantly, the integrity of tight junctions is crucial to prevent the paracellular transport of many molecules and ions, and its disruption is associated with pathological events. The cellular and molecular properties of brain ECs are essential for maintaining BBB permeability through an adequate ionic balance, conservation of the junctional structure and an adequate interaction with cells of the NVU (Cabezas et al., 2014).

To note, the cytoplasmic Ca^{2+} concentration ($[Ca^{2+}]_i$) of the endothelial layer and the extracellular ATP are essential for the balance of the BBB. Preventing $[Ca^{2+}]_i$ alteration can be useful in the protection of BBB against malfunctioning homeostasis (De Bock et al., 2013; Bynoe et al., 2015). On the other hand, ATP, acting on purinergic receptors, the metabotropic P2Y receptors and their ionotropic P2X counterparts in the endothelial membrane causing TJs degradation, via both Ca^{2+}-dependent and Ca^{2+}-independent pathways (Yang et al., 2016).

1.2.1.1 Tight Junctions

ECs of BBB are characterized by a unique phenotype distinguished by the presence of TJs and polarized transport systems. Notably, TJs constitute an

intercellular complex with three main functions: a barrier to diffusion of polar substances, a fence preventing the lateral diffusion of lipids and a base for intracellular signalling (Luissint et al., 2012).

TJs platform of brain ECs is composed by membrane proteins (occludin, claudins and junction adhesion molecules (JAMs)), which directly interact with cytoplasmic scaffolding proteins such as ZO proteins and other proteins like protein kinases and G-proteins (Vorbrodt and Dobrogowska, 2003).

Occludin (60 kDa) is a tetraspan integral membrane protein. It was the first integral protein discovered within the TJ of ECs. As a member of the TJ-associated marvel proteins (TAMP) uses the cysteine residues of its MARVEL transmembrane domain to mediate oligomerization in endothelial cells (Ikenouchi et al., 2005). This process is redox-sensitive and contributes to the redox-dependence of he TJ complex. In this context, oxidative stress conditions induced by inflammation or hypoxia-reoxygenation lead to TJs disruption (McCaffrey et al., 2008; Walter et al., 2009). Low extracellular electrical resistance and increased paracellular permeability characterize cell monolayers, lacking occludins (Zlokovic, 2008). Moreover, dephosphorylation of occludins contributes to increased BBB permeability in mice with experimental autoimmune encephalomyelitis (EAE), a model of multiple sclerosis (Morgan et al., 2007).

Claudins are a large family of more than 20 members expressed both in endothelial and epithelial cells. They form the TJ strand through the interactions between two extracellular loop of 2 claudins (Zlokovic, 2008). Cludin-3, -5 and -12 are mainly expressed in brain endothelial cells (Wolburg, 2006). As occludins, even claudins can be degraded by metalloproteinases (MMP-2 and MMP-9) after ischemic insult causing BBB disruption (Yang et al., 2007).

Besides occludins and claudins, also the junctional adhesion molecules (JAM), even if not essential, have a peculiar role in the TJ assembling and in the organization of cell polarity (Bazzoni, 2011).

TJ transmembrane proteins are linked to the cytoskeletal platform thanks to cytoplasmic proteins, which contribute to TJ integrity. Among them, membrane-associated guanylate kinase (MAGUK) family (ZO-1, ZO-2 and ZO-3) have been widely investigated (Hawkins and Davis, 2005). To note, ZO

proteins allow the anchorage of transmembrane TJ proteins to the cytoskeleton and drive the correct spatial distribution of claudins via the PDZ domains (Fanning et al., 2002). Decreased expression of zonula occludens 1 (ZO-1) in brain endothelial cells, during diabetes in rats, has been associated to BBB permeability increase. Furthermore, levels of MAGUK proteins can be modulated by caveolin-1 activity (Song et al., 2007).

Aside from transmembrane and cytoplasmic proteins, the cytoskeleton has a critical role in the normal formation of the TJ complexes along the BBB. Notably, the correct arrangement of actin filaments is fundamental to allow proper BBB function. Otherwise, the induction of stress to actin filaments, with consequent cytoskeleton reorganization, augments the BBB permeability (Shiu et al., 2007).

1.2.1.2 Adherens junctions

Intermixed with the TJs, the adherens junctions (AJs) are usually found. VE-cadherin and platelet endothelial cell adhesion molecule 1 (PECAM-1), also known as CD31, are the most studied. VE-cadherin are linked to the cytoskeleton through the armadillo protein, β-catenin (Bazzoni and Dejana, 2004). Changes in their expression contribute to increased permeability of BBB and to leukocyte migration in the CNS. Intriguingly PECAM-1 is fundamental for leukocyte migration across endothelium. Blocking CD-31 in brain pathologies characterized by leukocyte infiltration could be potentially of benefit (Zlokovic, 2008).

1.2.2 Astrocytes

Astrocytes are the most common cell type in the mammalian brain, co-forming the glia with oligodendrocytes and microglia. Astrocytes are essential for many metabolic processes in the brain such as the promotion of neurovascular coupling, the attraction of cells through the release of chemokines, K+ buffering, release of gliotransmitters, release of glutamate by calcium signaling, production of antioxidant compounds like glutathione (GSH), uptake of glutamate and γ-aminobutyricacid (GABA) (Cabezas et al., 2014).

Two structural proteins morphologically characterize astroglia: the intermediate filaments vimentin (Vim) and glial fibrillary acidic protein (GFAP). To note, they are up-regulated under CNS insults, leading a process called astrogliosis. Morphologically, astrocytes are characterized by a stellate shape with multiple ramifications, and become activated following brain injuries, degenerative diseases and chronic pain disorders (Di Cesare Mannelli et al., 2013; Hol and Pekny, 2015).

Two main types of astrocytes have been described in the CNS: protoplasmic astrocytes of the grey matter which envelope neuronal bodies and synapses, and fibrous astrocytes from the white matter that interact with the nodes of Ranvier and oligodendroglia (Cabezas et al., 2014).

Thanks to their terminals processes, known as endfeet, astrocytes share dynamic interaction the brain vasculature surface and neurons. By Ca^{2+} oscillations, astrocytic endfeet control both cerebral blood flow and neuronal activity (Zonta et al., 2003; Maragakis and Rothstein, 2006).

K^+ channels and aquaporin 4 (AQP4) expressed on astrocytic endfeet partecipate in the regulation of vascular ionic concentrations and protein transporters (Nag 2011). Moreover, gap junctions allow the communication between neighboring astrocytes, thus forming a functional syncitium with well-coordinated responses (Alvarez et al., 2013). In this context, this inter-astroglial gap junctions apparatus has been suggested to regulate vasodilation and vasoconstriction of capillaries (Alvarez et al., 2013). Furthermore, astrocytes can manage the development and maintenance of BBB characteristics in ECs through the release of growth factors like VEGF, glial cell line-derived neurotrophic factor (GDNF), basic fibroblast growth factor (bFGF), and ANG-1 (Alvarez et al., 2013; Wong et al., 2013). Particularly, these growth factors are essential in the polarization of transporters, the formation of tight junctions as well as proper neuronal functions (Wong et al., 2013). On the other hand, during pathological conditions, reactive astrocytes alter the normal secretion of factors and other molecules driving vascular permeability and CNS damage (Argaw et al., 2009).

1.2.3 Pericytes

Pericytes are rounded and isolated cells that are in close contact with endothelial cells (Muoio et al., 2014). Morphologically, pericytes tend to be aligned with the vessel axis and extend protrusions enwrapping ECs in different patterns, along the abluminal surface (Armulik et al., 2010). A continuous basal membrane envelops both pericytes and ECs all together, and, at the same time, separate pericytes from astrocytic endfeet (Sá-Pereira et al., 2012). Typically, the ratio between pericytes and endothelial cells is around 1:3 (Shepro and Morel, 1993). Pericytes can be granular (95% of total pericytes) or agranular depending on the presence or the absence of lysosome granules in the cytoplasm. Intriguingly, alteration in granular pericytes have been linked to amyloid deposition and lipid accumulation suggesting a correlation between pericyte alterations and neurodegenerative pathologies such as Alzheimer disease (Castejón, 2011).

Functionally, pericyte are essential in the regulation of the NVU. Their relevant functions include stromal regeneration, neovascularization, control of ECs proliferation and promotion of neural stem cell properties (Lange et al., 2013). The association between pericytes and the other components of the BBB is achieved by the secretion of platelet derived growth fator-B (PDGF-B), another angiogenic factor such as VEGF, the angiopoietins (Angs) and the transforming growth factor-β (TGF-β) (Armulik et al., 2010). For example, PDGF-B secreted from ECs binds with the corresponding receptor (PDGFR-B) on pericytes, regulating recruitment of pericytes as well as their proliferation (Bell et al., 2010; Dalkara et al., 2011; Winkler et al., 2011). To note, it has been shown that the activation of PDGFR-B signalling allow both pericytes and astrocytes to manage brain vasculogenesis and BBB maintenance (Bonkowski et al., 2011). In this context, the interactions between pericytes and astrocytes are of greater importance. Together, they preserve and regulate the expression of the endothelial TJs like occludin, claudin and ZO-1 (Haseloff et al., 2005; Wolburg et al., 2009; Bonkowski et al., 2011). The communication between astrocytes and pericytes is important for the brain physiology, although further studies are needed in order to better understand the contributions of these interactions in the brain pathology.

Pericytes are contractile and, together with astrocytes, contribute to the regulation of blood flow by controlling capillary diameter (Peppiatt et al.,

2006; Hamilton et al., 2010; Dalkara et al., 2011). In cell culture, pericytes selectively express α-smooth muscle actin, which is not expressed in ECs, and they do not express neither GFAP, expressed by astrocytes, nor vWF, expressed by ECs. Furthermore, studies in mice have suggested that newborn capillaries recruit pericytes during the development and since when they get function, pericytes are the key for regulate both development of the BBB and transport across of the BBB (Armulik et al., 2005, 2010; Daneman et al., 2009, 2010; Kim et al., 2009). On the other hand, pericytes lost lead to local alteration of the blood flow and to BBB leakage (Armulik et al., 2010; Bell et al., 2010).

1.2.4 Extracellular Matrix

The extracellular matrix (ECM) is a crucial structural component of the BBB. It anchors the endothelium throughout the interaction between matrix protein such as laminin and endothelial integrin receptors. The ECM is mainly composed of proteoglicans, hyaluronic acid, hyaluronan, lecticans and tenascins, which permit the paracellular diffusion in the NVU (Wong et al., 2013). The ECM disruption is strongly associated with the increase of the BBB permeability during pathological states. For example, it is well known that, during ischemia, that the activation of the matrix metalloproteinases (MMPs) MMP2 and MMP9 lead to the basement membrane suffering which in turn lead to the neighbor glial activation (Lau et al., 2013).

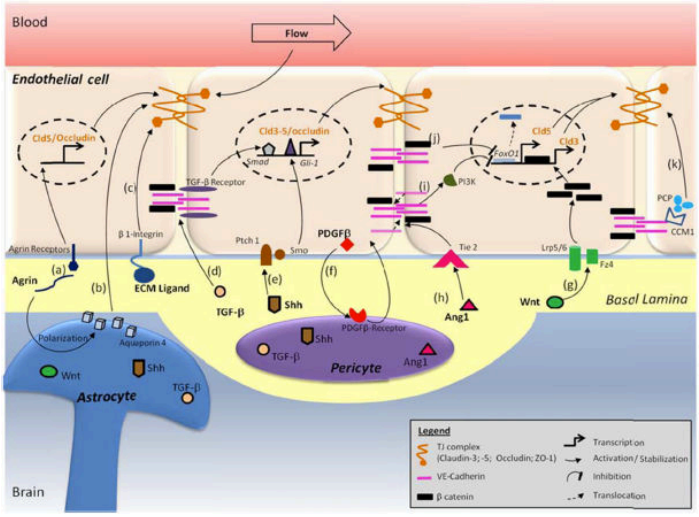

Figure 2. Schematic representation of the NVU and modulation of TJs

1.3 BBB under pathological conditions

Brain disorders and neurological disease caused by meningitis encephalitis, traumatic brain injury, Alzheimer's disease and small vessel disease such as diabetes or hypertension may modulate both morphology and function of BBB. Recently, it has been suggested that also pain disorders including migraine, inflammatory pain and neuropathic pain can trigger change of the BBB physiology (Rosenberg, 2012).

1.3.1 BBB and neuropathic pain

Focusing the attention on pain-induced BBB alterations, one of the first works on this field has illustrated that in a model of neuropathic pain, the chronic constriction of the sciatic nerve impaired the blood spinal cord barrier (BSCB) integrity along with astrocytic activation in the spinal cord (Godh and Sharma, 2006). In another investigation, the authors found that the application of capsaicin to the healthy afferent C-fiber was capable to elicit both BBB and BSCB permeability, as assessed by Evans blue dye extravasation, allowing the concept that the TRPV1- expressing fibers could be responsible for the BBB/BSCB breakdown (Beggs et al., 2010).

BSCB permeability can be altered even after a partial sciatic nerve ligation, where the passage of different sized tracers was prominent in the lumbar than in the thoracic spinal cord. Isolated microvessels from the lumbar spinal cord parenchyma revealed down regulation of the tight junction proteins ZO-1 and occludin (Echeverry et al., 2011). Pain caused by L4 spinal nerve lesions in rat models lead to BSCB disruption accompanied by astrocytic activation in the gray matter of the lesioned side (Gordh et al., 2006).

A distinction should be made between BBB "permeabilization" and BBB "disruption" in experimental animal models. The term permeabilization refers to a transient process with increased permeability but no (or reversible) TJs opening or altered efflux transport. On the other hand, the disruption of BBB is a long-term often–irreversible phenomenon followed by extravasation of Evans blue and albumins in the spinal cord or brain parenchyma (Sharma and Sharma, 2010).

Neuropathic conditions where the inflammatory component is more expressed lead to BBB permeabilization and not to BBB disruption. Both the injection of λ-carrageenan and the complete Freund's adjuvant (CFA) in the hindpaw paw of the rat increased the immediate brain uptake of [^{14}C] sucrose and the transitory down regulation of ZO-1 in brain microvessels. On the other hand Evans blue, injected to assess the BBB integrity, was not found in the CNS parenchyma (Huber et al., 2002; Radu et al., 2013).

Better knowledge of BBB's structural and functional alterations during neuropathic pain events could generate new insights into understanding pathophysiological mechanisms at the basis of various clinical pain disorders. This ultimately would permit the discovery of new and safer remedies for the treatment of neuropathic pain.

In this context, the signalling between astrocytes and endothelial cells is altered under pathological conditions (Abbott et al., 2006). However, the overall crosstalk within the NVU is altered during pathological alterations.

1.4 Oxaliplatin - use and toxicity

Colo-rectal cancer (CRC) represents the third most common cancer worldwide and it is currently a public health priority (American Cancer Society, 2009). It has been estimated that, in 2017, 95520 new cases of colon cancer and 39910 of rectal cancer will be diagnosed in the United States (Siegel et al., 2016). Approximately, 80% of patients are diagnosed at a stage in which the surgery is the most common therapeutic modality. The rate of 5-year survival with stage II and III colon cancer (respectively 80% and 60%) after surgical procedure demonstrates that many patients will have recurrences and will die of this pathology (Hayat et al., 2007). However, also patients with CRC and treated with adjuvant therapies and surgery show nearly 25% of recurrences (Sauer et al., 2004). Between 50s and 90s, fluororacil (5-FU) has been the only clinically relevant agent against metastatic CRC. Although 5-FU significantly increased the survival and ameliorated the quality of life of patients with CRC, treatment with this agent had reached a plateau in efficacy. In this context, the introduction of oxaliplatin and irinotecan has changed the management of patients with advanced CRC, during the 20 past years. Several combinations of

regimens of oxaliplatin and infusional 5-FU/leucovorin (FOLFOX) or capecitabine (XELOX) have been developed (Grothey and Goldberg, 2004) and actually they appear as important options in the adjuvant treatment of colorectal cancer. Notably, the addition of oxaliplatin to 5-fluorouracil (5-FU) and leucovorin (LV) proved to be a significant improvement in the treatment of metastatic colon cancer (Rothenberg et al., 2003). This combination, called the FOLFOX regimen, has become part of the worldwide standard of care for the adjuvant and the palliative treatment of the disease (Lonardi et al., 2016).

The clinical development of oxaliplatin-based regimens started in the 1990s and, along the years, several different combinations of 5-FU, leucovorin, and oxaliplatin, collectively named FOLFOX, have been studied. De Gremont and colleagues found for the first time that this combination, called FOLFOX2, produced a response rate (RR) of 46% for patients in whom prior treatment with 5-FU and leucovorin alone had failed (de Gramont et al., 1997). Following these results, a different regimen with a lower dose of oxaliplatin (85 mg/m^2) was tested in a clinical trial in order to reduce the neuropathy experienced by patients under treatment with the FOLFOX2. However the RR registered with FOLFOX3 decreased (20%). Later, a regimen administered twice a month also was tested; this regimen consisted of oxaliplatin (85 mg/m2 on day 1), leucovorin (200 mg/m^2 in a 2-hour infusion on days 1 and 2), and 5-FU (400 mg/m^2 bolus and 600 mg/m^2 by a 22-hour infusion on days 1 and 2) has known as FOLFOX4. The response rate was mildly higher: 23.5%. Recently, FOLFOX6 and its modified version (mFOLFOX6) have reached general acceptance among oncologist (Allegra et al., 2009; Tournigand et al., 2004). In mFOLFOX6, oxaliplatin is administered as in FOLFOX4 (85 mg/m2 on day 1) whereas 5-FU is administered as a bolus (400 mg/m2) on day 1 and as a continuous infusion over 46 hours (2400 mg/m^2), and leucovorin is given on day 1 (400 mg/m^2). Subsequently, the FOLFOX7 was developed to maximize the dose of oxaliplatin (130 mg/m^2) in combination with the simplified infusion schedule of 5-FU already used in the FOLFOX6. The FOLFOX7 emerged as the regimen with the highest RR (Maindrault-Goebel et al., 2001).

Already used in Europe, the FOLFOX regimens were worldwide accepted as first-line treatment for the management of colorectal cancer after the N9741

trial, determined the higher efficacy of FOLFOX4 with respect to both 5-FU and leucovorin alone and leucovorin "bolus" plus irinotecan (Goldber et al 2004, de Gramont et al., 2000). Actually, the FOLFOX4 has become the most used regimen in the United States, although the FOLFOX7 regimen showed higher RR and reduced neurologic and hematologic toxicities. In this context, the OPTIMOX study demonstrated that FOLFOX7 and FOLFOX4 had similar efficacy if used as first-line option in the treatment of advanced CRC. In addition, the OPTIMOX study highlighted that the reintroduction of oxaliplatin in patients with stable disease does not compromise survival (de Gramont et al., 2004). Furthermore, oxaliplatin has become an essential component of adjuvant therapy in patients with metastatic liver lesions from CRC (Nordlinger et al., 2008). In an international clinical trial, known as MOSAIC trial, Andrè and colleagues determined if the efficacy of oxaliplatin in the metastatic environment could translate into benefit in earlier stages (II and III) of colon cancer. In this study, FOLFOX4 improved 3-year disease-free survival (DFS), compared with 5-FU and leucovorin alone (78.2% vs. 72.9%; hazard ratio [HR] 0.77; *P* = .002). The final results of the MOSAIC trial showed also that adding oxaliplatin to the 5-FU and leucovorin backbone improved the 5-year DFS (73.3% vs. 67.4%; HR 0.80; P = .003) and 6-year overall survival (78.5% vs. 76.0%; HR 0.84; P = .023) in the adjuvant treatment of stage II or III colon cancer (Andrè et al., 2004). In conclusion, the regimens containing oxaliplatin should be strongly considered in patients in whom significant difference in overall survival was found in subgroup analysis (Andrè et al., 2009).

Currently, oxaliplatin represents a valid option for the treatment of several gastrointestinal carcinomas and it is indicated for localized oesophageal carcinoma (NCCN, 2009). Additionally, the use of platinum derivative together with irinotecan and 5-FU has evidenced improved survival in advanced pancreatic cancer if compared with single-agent gemcitabin (Conroy et al., 2010).

1.4.1 Mechanism of action

Oxaliplatin is a diamine cyclohexane (DACH) platinum (Pt) derivative that is active in several solid tumour types, especially in some cisplatin-resistant cancers (Machover et al., 1997). It belongs to the category of drugs not cell cycle specific (CCNS), which are able to interact with tumour cells irrespective of the phase of the cell cycle. The mechanism of action of this drug is similar to that of the platinum derivative. Firstly, it has to be converted in the active aqueous form passing through the mono- and di-chloride forms. Thanks to this conformation it can bind the N atoms of the nitrogen bases of DNA, leading to apoptosis, as well as it is able to attach the sulfhydryl groups of proteins (Di Francesco et al., 2002). Therefore, oxaliplatin irreversibly interact with molecules such as methionine (Met), cysteine (Cys) and reduced glutathione (GSH). To note, decreased levels of reduced GSH alter the cellular oxidative equilibrium. The anti-tumour efficacy of oxaliplatin is mainly due to the formation of the adducts DACH-Pt-DNA, that may be created within the same filament or between different filaments. These adducts, in turn, deforms the DNA structure and subsequently, arrest the synthesis and damage repair processes, so contributing to cell death by apoptosis. Since the DACH core, oxaliplatin interacts more efficiently with proteins, if compared with other Pt-derivatives. Lesions induced by oxaliplatin are, therefore, more harmful than those caused by cisplatin or carboplatin (Di Francesco et al., 2002).

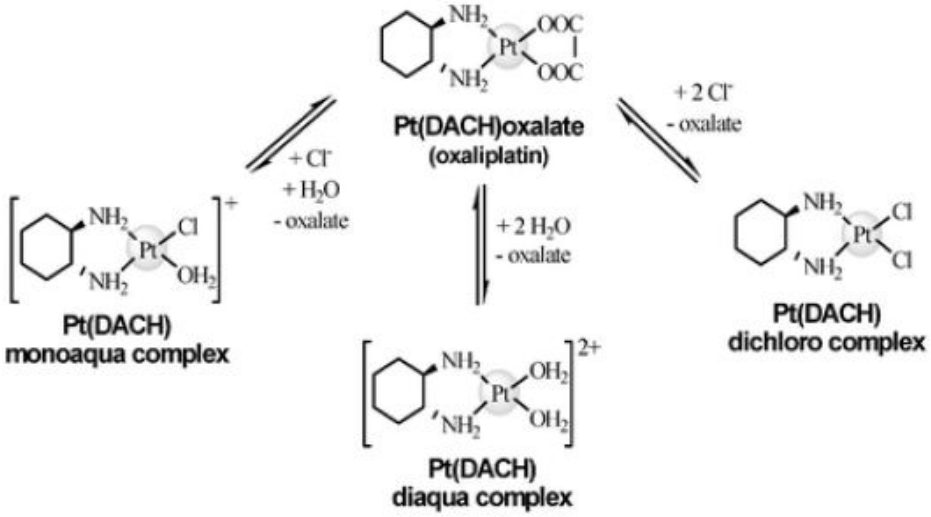

Figure 3. Hydrolisis of oxaliplatin (Esteban-Fernandez et al., 2010).

1.4.2 Oxaliplatin-induced neuropathy

Oxaliplatin is better tolerated than conventional carboplatin/cisplatin-based regimen, especially among older patients (Jing et al., 2015). Nonetheless a

major limitation to the widespread use of oxaliplatin is represented by its neurotoxicity, which leads to sensory neuropathy. The neurotoxicity can manifest with distinct syndromes: an acute one that onsets shortly after infusion, and a dose-limiting, cumulative sensory neuropathy (Saif and Reardon, 2005). The incidence of acute platinum-induced neuropathy ranges from 65% to 100%, and the symptoms are usually reversible within hours or days. It has been associated with significant peripheral nerve hyper-excitability, which suggests an immediate pharmacologic rather than structural basis for acute symptoms (Webster et al., 2005). It has been suggested that the oxaliplatin-induced neurotoxicity could be due at least in part to the neural sodium channel dysfunction (Park et al., 2000). The action on a peculiar population of sodium channels (calcium-dependent sodium channels) is produced by oxalate, a cytotoxic metabolite of the Pt-derivative, which acts as calcium chelator (Grolleau et al., 2001). Oxalate alters the intracellular divalent cation equilibrium impairing neuronal homeostasis (Gamelin et al., 2002).

Otherwise, the cumulative neurotoxicity may affect up to 80% of patients (Grothey and Goldberg, 2004), causing paresthesia, dysesthesia, pain combined with a glove and stocking distribution sensory loss, impairing their functional capacity and compromising the treatment plan (Kannarkat et al., 2007; Wolf et al., 2008). Moreover, prolonged affected proprioception may result in ataxic gait (Avan et al., 2015). To note, moderate-severe grade neuropathy (grade-3 neuropathy) occurs in up to 30% of patients treated with cumulative oxaliplatin doses, ranging from 765 to 1020 mg/m^2, and in 50% of patients treated with higher doses (Kalofonos et al., 2005; Argyriou et al., 2007; Land et al., 2007).

Information regarding the molecular basis of oxaliplatin-induced neuropathy is still insufficient. Severe alterations occur in the peripheral nervous system (PNS) where nerves and dorsal root ganglia are strongly affected. To note, oxaliplatin has a low capability to cross the BBB (Jacobs et al., 2005; Huang et al. 2016) (See the paragraph below). Otherwise, the central nervous system (CNS) negatively reacts with a maladaptive plasticity of both neurons (Di Cesare Mannelli, 2015a; Renn et al., 2011) and glial cells (Di Cesare Mannelli et al., 2013; Di Cesare Mannelli et al., 2014).

To the best of our knowledge, morphological examination revealed that the primary target of oxaliplatin, and more in general of platinum compounds, are the dorsal root ganglia (DRGs) where the accumulation of the antineoplastic agent, following repeated administrations, triggers nuclear damage (Cavaletti et al., 2001; Di Cesare Mannelli et al., 2013). However, molecular modifications occur both in DRGs and in the sciatic nerve with downregulation of the phosphorylated-neurofilament H (p-NF-H), which have an essential role in the axoplasmic transport (Nixon et al., 1987). Moreover, elevated expression of ATF3/cAMP-responsive element binding protein (CREB) family (Carlton et al., 2009) has been shown both in the DRG neurons and in the Schwann cells of the peripheral nerve of oxaliplatin-treated rats (Di Cesare Mannelli et al., 2013). On the other hand, the CNS is strongly involved in pain sensitization. Consistently with the alteration of the painful threshold, electrophysiological measurements have evidenced an overall nociceptive-specific neuron hyper-excitability in the dorsal horn of the spinal cord (Di Cesare Mannelli et al., 2015a; Renn et al., 2011). Nevertheless, besides the neuronal maladaptive plasticity, repeated treatment with oxaliplatin lead to intense molecular and morphological changes in the CNS. Increasing levels of the oxidized forms of DNA and proteins have been found in the spinal cord of oxaliplatin-treated animals (Di Cesare Mannelli et al., 2012). Glial cells of the CNS are mainly involved in the development and maintenance of neuropathic pain states (Marchand et al., 2005; Wieseler-Frank et al., 2004). Microglia and astroglia strongly react in both spinal and supraspinal areas in response to repeated injections of oxaliplatin. However, while microglial activation usually ends within few days, the astrogliosis continuously accompany the treatment with the antineoplastic agent, suggesting a more complex involvement of astrocytes in pain maintenance (Di Cesare Mannelli et al., 2013; Pacini et al., 2016).

Although the evidences collected up to now about the neurotoxicity evoked by the platinum-derivative, effective treatments against oxaliplatin-induced neuropathy are lacking. Duloxetine is the only recommended intervention. Nevertheless, it is not completely effective and did not work for everyone (Smith et al., 2015). Tricyclic antidepressants are not recommended but clinicians may use them after discussion with patients about the limited effectiveness. The antiepileptic drugs, pregabalin and gabapentin, have not

well established efficacy as resulted from clinical trials but, given the limited options for managing neuropathy, their clinical use is encouraged (Hershmann et al., 2014).

1.5 Oxaliplatin and BBB

Few studies have so far analysed the ability of oxaliplatin to cross the BBB. Surely, the difficulty of dosing the Pt-compound over the barrier has been an important limit of this study. Additionally, the attention has been focused on the penetration in the acute phase rather than following repeated administration.

In a nonhuman primate model, the platinum concentration was measured in the CSF using the atomic absorption spectrometry. Oxaliplatin was given at the dose 5 mg kg^{-1} *i.v.* (intravenously) over 2 hours (human equivalent, 110 mg/m^2) and CSF was collected over 24 hours from injection. Data revealed that oxaliplatin peaked in the CSF at 0.2 μM and the AUC was <5% of the exposures achieved in the plasma (Jacobs et al., 2005). In a second study, Jacobs and coworkers confirmed the low capability to penetrate the brain (<5%) even by the using of the microdyalisis technique for collecting samples from extracellular fluid (ECF) of brain tissue, even though the correlation between CSF and ECF measurements was poor (Jacobs et al., 2010). More recently, similar results were obtained in a rat model (Huang et al., 2016). The analysis, carried out with the inductively coupled plasma–mass spectrometry, of the oxaliplatin in the CSF after a single administration (4 mg kg^{-1}, *i.p.* (intraperitoneally)) corroborated the previous data. The concentration of the platinum derivative was 6.6 nM. However, the same amount, directly injected in the CSF was able to cause thermal hyperalgesia in the rat and to initiate the inflammatory response in the spinal cord region (Huang et al., 2016). These data, even if underdeveloped, may suggest that the acute painful neuropathy induced by systemic administration of oxaliplatin could be due to the direct penetration of the Pt-compound in the CNS (Huang et al., 2016).

On the other hand, data regarding the penetration after repeated treatment are lacking, even though limited accumulation is observed in plasma after repeated cycles (five consecutive cycles at 85 or 130 mg/m^2 every 3 weeks). In humans,

the plasmatic concentration of inorganic platinum, after a single *i.v.* injection of 85 mg/m^2, is on average about 3 μg/ml (Graham et al., 2002; Han et al., 2013). Preclinical data have evidenced that the inorganic platinum plasmatic levels after 21 days of treatment in the rat receiving a cumulative dose comparable to the human being, is 3.573±0.217 μg/mL (corresponding to oxaliplatin 7.274±0.552 μg/ml or 18.3 μM) in line to human plasma concentration (Zanardelli et al., 2014).

Within the BBB, unsaturated active efflux transporters with elevated specificity for oxaliplatin might account for the low concentration of platinum in the CNS (Sawchuk and Elmquist, 2000; Kusuhara and Sugiyama, 2005). Otherwise oxaliplatin could exploit specific influx transporters to cross the BBB. Among them, organic cationic transporters (OCT1 and OCT2) have been considered the major responsible of the oxaliplatin cytotoxicity (Zamboni et al., 2002; Zhang et al., 2006), although their presence on the plasma membranes of the BBB endothelial compartment is still under debate (Jacobs et al., 2010; Wu et al., 2015). Furthermore, the copper transporters also allow the oxaliplatin entry into the cell. Treatment with oxaliplatin of different human colorectal cancer cell lines overexpressing the copper uptake transporter 1 (CTR1) is related to an increase of cellular mortality (Cui et al., 2017). However, if the presence of Cu^{2+} transporters on the BBB is known for the regulation of the copper homeostasis over the barrier, endothelial cells have both channels involved in the influx and transport proteins that participate in Cu^{2+} efflux (ATP7A and ATP7B) (Choi and Zheng, 2009; Li et al., 2016).

1.6 Gap Junctions

The gap junctions are made up of low-strength channels that establish direct communication between cytoplasm of two adjacent cells. These connections allow the passage of currents and small solids (<1.4 nm in diameter) such as ions and second messengers (e.g. Ca^{2+} and inositol triphosphate ($InsP_3$)). These channels are formed by the attachment of two hemichannel, each of which is provided by one of the two cells that take part in the junction. Each hemichannel is constituted by the assembly of 6 conjugates (proteins), which are organized around a central pore. The monomer (connexin) consists of 4

transmembrane domains that have the intracytoplasmic C-ter and N-ter ends; the transmembrane domains TM1 TM2, TM3 and TM4 are interconnected by two extracellular loops, while TM2 and TM3 domains are connected by an intracytoplasmic loop. The latter and the C-ter extremities are the most variable portions of the protein, while the extracellular domains possess a variety of Cys, which by Cys-Cys bridges firmly join the above domains. To date, 20 conjugate isoforms are known which are named by the apparent molecular weight. Cells generally express more than one isoform, and the hemichannel can thus be formed by either a single contingent (homomeric channels) or by the association of different connectors (heteromeric channels). It is important to point out that each contingent has conductance, permeability and adjustment characteristics (Saez et al., 2003).

The operating mode of the connexins is not limited to their coupling; it has been demonstrated that hemichannels may not fit together and release paracrine signals such as ATP, NAD^+, prostaglandins or NO in the extracellular space (Figueroa et al., 2013).

1.6.1 Pannexin hemichannels

Gap junctions are common to all multicellular life forms, but despite this functional conservation a partition exists at the molecular level. Invertebrates display direct cell-cell coupling through gap junction channels but they have not connexions in their system (Cruciani and Mikalsen, 2006). In contrast, functional gap junction molecules with no sequence homology to connexins were identified in invertebrates (such as insects and nematodes) and they were named innexins (Phelan et al., 1998). These vertebrate homologs were hence called pannexins, from the Latin pan which means ‘throughout’ or ‘all’ (Baranova et al., 2004; Panchin et al., 2000) but do not share any homology with their all-vertebrate counterparts, connexins (Yen and Saier, 2007). Three pannexin genes have been identified in genomes of man and mouse: PANX1, PANX2 and PANX3. These genes are conserved in invertebrate species such as vermin and insects. Despite the difference in the gene sequence, pannexins proteins have the same topology as connexins: they are tetra-span proteins that have their C- and N-terminus located intracellularly (Baranova et al., 2004; Bruzzone et al., 2003). Before further processing and assembling, pannexin

mRNA translates in the ER. Here the protein is assembled, transferred to Golgi apparatus and then delivered to the cell surface (Bhalla-Gehi et al., 2010). Furthermore, unlike innexins and connexins, pannexins are glycosylated, which negatively affects hemichannel docking (Boassa et al., 2007; Penuela et al., 2009). Pannexin western blots reveal three bands corresponding to G_0, a nonglycosylated state; G_1 that marks a high mannose-type glycoprotein and G_2, the fully processed glycoprotein that is present in the plasma membrane (Boassa et al., 2007). The degree of glycosylation differs between tissues: in endothelium only G_0 Panx1 is identified (Boassa et al., 2007), and this non-glycosylated protein was also found on the cell surface of human embryonic kidney cells (Penuela et al., 2009). The exogenous expression of Panx1 and Panx2 in Xenopus oocytes resulted in the formation of homomeric Panx1 hemichannels or heteromeric Panx1:Panx2 channels, activated by depolarization. Moreover, Locovei and colleagues discovered that erythrocytes, that do not express connexins, release ATP via Panx1, thus emphasizing the functional role of these hemichannels (Locovei et al., 2006). Pannexin hemichannels can be opened by different triggers such as depolarization, $[Ca^{2+}]_i$ increase, cleavage by caspase-3 and mechanical stress (Bruzzone et al., 2003; Thompson et al., 2006; Dahl, 2015). Moreover it is suggested that Panx1 as hemichannel, could form a large pore (through which molecules up to 1 kDa can pass) upon activated by the purinergic receptor $P2X_7$ ($P2X_7R$) (Locovei et al., 2007). It has been demonstrated that Panx-1 co-immunoprecipitates with $P2X_7R$ and inhibition of Panx1 prevents $P2X_7R$-mediated dye uptake. Moreover, as large pore, Panx1 could play role in the formation of the inflammasome (Pelegrin and Surprenant, 2006).

1.7 Pannexins and Connexins in the NeuroVascular Unit

1.7.1 Pannexin and connexins at the vascular wall

Connexins and pannexins are expressed throughout the cardiovascular system. The expression levels within the vascular tree are dependent upon vessel type, localization within the vessel, and the species being examined. Cx43 is the most studied connexin. It has been found in ECs of arteries and veins (Pogoda et al., 2014; Kaneko et al., 2015). Cx37 and Cx40 are also found broadly across the vascular network (Brisset et al., 2009; Gaete et al., 2014; Miquerol et al.,

2015). Otherwise less is known about localization of Cx32, Cx45 and Cx47. On the other hand, pannexin channels are expressed throughout the body. Recent data show that Panx1 is expressed in mouse ECs of arteries, arterioles and venules as well as in isolated human cells lines, like human saphenous vein ECs (HSaVECs), HUVECs and also an immortalized brain EC line (Lohman et al., 2012a; Kaneko et al., 2015; Lohman et al., 2015). Intriguingly, in the last decade the role of connexin hemichannels and pannexin channels in the vascular inflammation has been deeply investigated. The regulation of BBB ECs under inflammatory conditions was linked to connexin hemichannel opening; specifically bradykinin, a pro-inflammatory agent, evoked an increase in BBB permeability in rats through the activation of intracellular Ca^{2+} oscillations in ECs by a pathway sensitive to the Cx43 inhibitor Gap27, indicating the involvement of hemichannel opening and purinergic signalling in response to bradykinin (De Bock et al., 2011). In another study, both connexin hemichannels and pannexin channels were studied in a blood–brain barrier (BBB) model system (Kaneko et al., 2015). Using the human cerebral microvascular endothelial cell line hCMEC/D3, conditions mimicking acute ischemic stroke led to the opening of both Cx43 hemichannels and Panx1 channels, as observed by increased dye uptake and calcein efflux, respectively. Pharmacological inhibition with CBX or 18α-GA and knockdown with either Cx43 siRNA or Panx1 siRNA prevented the dye uptake and calcein efflux (Kaneko et al., 2015). Furthermore, connexin and pannexin openings in ECs of BBB contribute in ischemia/reperfusion conditions (Robertson et al., 2010; Wei et al., 2015).

1.7.2 Pannexins and connexins in astrocytes and neurons

Connexins and pannexins are widely expressed also in the other cells of the NeuroVascular Unit, particularly at astrocytic and neuronal level. In this context, astrocytes are functionally as well as metabolically coupled with neurons (Koehler et al., 2009). They are furnished of several receptors for neurotransmitters such as ATP and glutamate providing mechanicistic bases for synaptic activity (Anderson and Nedergaard, 2003; Leybaert, 2005). To note, astrocytes can release key molecules as the above-mentioned ATP and glutamate providing important signalling pathways in the neurovascular

coupling. On the other hand, neuron, in addition to have receptors for these substances, they also express connexins and pannexins hemichannels, both permeable to ATP (Schock et al., 2008; Thompson et al., 2006). In astrocytes, both glutamate and ATP increase the $[Ca^{2+}]_i$. This signals led astroglial cells to coordinate neuronal activity and vasodilatation. Notably $[Ca^{2+}]_i$ increase at the astrocytic end-feet level results in the release of factors as prostaglandins, epoxyeicosatrienoic acid and K^+ (Koehler et al., 2009; Zonta et al., 2003; Filosa et al., 2004). Noteworthy, $[Ca^{2+}]_i$ increase is concomitant to augmented Cx43 and Panx1 hemichannel activities (Locovei et al., 2006, De Vuyst et al., 2009).

1.8 Pannexin and pain

Pannexin channels and, in particular, Panx1 opening are strongly involved in neurological disorders such as epilepsy and stroke (Kim and Kang, 2011). Otherwise, only recently researchers investigated a relationship between Panx1 and pain, although the Panx1 involvement in the release of ATP and glutamate are related to pain (Bennett et al., 2009). Evidence from animal models indicates that Panx1 plays a pivotal role in several types of pain, including trigeminal hypersensitivity, spared nerve injury- and chemotherapy-induced neuropathic pain (Hanstein et al., 2016; Zhang et al., 2015; Di Cesare Mannelli et al., 2015b).

In nervous cells, Panx1 is important in releasing both ATP and glutamate once recruited by the $P2X_7$ receptor under pathological conditions. Long lasting opening of the channel, usually closed at resting membrane potential, causes aberrant ionic current and dysregulation of neuronal firing by Ca^{2+} increase (Kim and Kang, 2011). However, in neuronal as well as non-neuronal cells (i.e. astrocytes), Panx1 could open, subsequently to extracellular K^+ or intracellular $Ca2^+$ increases, enabling the hemichannel in the release of large amount of ATP, thus, participating in pain chronicity (Spray and Hanani, 2017). In this context, a recent study highlighted the involvement of the glial Panx1 in a mouse model of chronic orofacial pain. In that model, the deletion of Panx1 in GFAP-positive cells completely prevented hypersensitivity, whereas deletion of neuronal Panx1 only affected baseline sensitivity and the duration of hypersensitivity, addressing an important role for non-neuronal Panx1 in the

pain transmission.

Other studies performed on rodents treated with Panx1 inhibitors have indicated that these channels are likely involved in both peripheral and central sensitization (Bravo et al., 2014; Zhang et al., 2015). The selective Panx1 inhibitor ^{10}Panx and the non-specific carbenoxolone decreased pain hypersensitivity in sural nerve transected animals (Bravo et al., 2014). Moreover, in mice in which $P2X_7R$ with defective C-terminal tail have impaired pore formation and coupling to Panx1, less allodynia was shown than in mice with the pore-forming $P2X_7R$; in humans genetic association between lower pain intensity and hypofunctional $P2X_7R$ with low pore-forming capability was found (Sorge et al., 2012). In another study, Panx1 expression dramatically increased in L4-L5 dorsal root ganglia (DRG) of spinal nerve ligated rats. The inhibition of Panx1 decreased the nerve injury enhanced hypersensitivity in animals (Zhang et al., 2015).

Regarding to chemotherapy-induced neuropathy, recently, it has been found that oxaliplatin treatment induces Panx1 channel recruitment by $P2X_7R$ on the nerve terminals of cerebral cortex increasing the glutamate release from cortical glutamatergic neurons. Both $P2X_7$ and Panx1 inhibitors intrathecally (i.t.) infused at spinal level decrease oxaliplatin-induced pain. Particularly, the intrathecal infusion of Panx1 channel relieved oxaliplatin-dependent alteration on pain threshold (induced by noxious and non-noxious stimuli) in a dose-dependent manner (Di Cesare Mannelli et al., 2015b).

2. Aim of the study

The aim of this study is to evaluate the interference of oxaliplatin with the BBB system in a rat model of oxaliplatin-induced neuropathy and in a rat brain endothelial cell line (RBE4).

As first, to investigate the possible alteration of the NVU environment, immunofluorescent stainings will be performed to detect IgG extravasation and reactive astrocytes in the lumbar BSCB of rats daily treated with oxaliplatin (2.4 mg kg^{-1}, *i.p*) for 14 days. Moreover, possible changes in permeability of BBB/BSCB of specific brain and spinal cord areas crucially involved in the oxaliplatin-induced neuropathic pain sensitization (prefrontal cortex, somatosensory area S1 and lumbar spinal cord) will be analysed by the *i.v.* injection of 10 kDa dextran texas red at different time points (days 1, 7 and 14) of chemotherapy treatment.

Further, aimed to deeply look into the altered machinery of the endothelial compartment of the NVU, we will set up an *in vitro* model which could reproduce the vascular wall of the BBB by the using RBE4 cells. The vitality assay will allow to choose concentration of oxaliplatin that slightly affect the RBE4 viability in 8-24 h period of treatment, in order to mimic a damage that does not irreversibly alter the endothelial compartment of the NVU.

Since oxidative stress is a remarkable feature of oxaliplatin-induced neurotoxicity (Zanardelli et al., 2014), the state of organelles, endoplasmic reticulum (ER) and mitochiondrion, susceptible of redox balance changes, will be evaluated. Respectively, western blot analysis will allow to measure the expression of glucose-regulated protein (GRP78) whose levels are altered during ER stress conditions (Wang et al., 2009), while the immunofluorescent staining of cytochrome C will let us to detect possible mitochondria alterations (Kim et al., 2006). Additionally, the expression of caspase-3 and BAX will be measured to further investigate metabolic and apoptotic pathways.

Morevover, because of the cytoplasmic Ca^{2+} of the endothelial layer and the extracellular ATP are essential for the balance of the BBB, and their variations could be harmful for the NVU homeostasis (De Bock et al., 2013; Bynoe et al., 2015), changes of both $[Ca^{2+}]_i$ and extracellular ATP will be evaluated. Furthermore, the analysis of TJ complex arrangement by the immunofluorescence staining of ZO-1 and the cytoskeletal protein F-actin will let to investigate changes in the RBE4 permeability.

Finally, since Ca^{2+} oscillations and ATP signalling are based on fast mechanisms, their variations, particularly focusing on the analysis of Ca^{2+} pathways, as well as ZO-1 and F-actin localization will be evaluated after short treatment with oxaliplatin (10 min).

3. Materials and methods

3.1 Animals

Male Sprague Dawley (SD) rats (Envigo, Varese, Italy) weighing approximately 200 to 250 g and male CD-1 albino mice (Envigo, Varese, Italy) weighing approximately 22-25 g at the beginning of the experimental procedure, were used. Animals were housed in CeSAL (Centro Stabulazione Animali da Laboratorio, University of Florence) and used at least 1 week after their arrival. Four rats were housed per cage (size 26 × 41 cm) and ten mice were housed per cage (size 26 × 41 cm); animals were fed a standard laboratory diet and tap water ad libitum, and kept at 23 ± 1 °C with a 12 h light/dark cycle, light at 7 a.m. All animal manipulations were carried out according to the Directive 2010/63/EU of the European parliament and of the European Union council (22 September 2010) on the protection of animals used for scientific purposes. The ethical policy of the University of Florence complies with the Guide for the Care and Use of Laboratory Animals of the US National Institutes of Health (NIH Publication No. 85-23, revised 1996; University of Florence assurance number: A5278-01). Formal approval to conduct the experiments described was obtained from the Animal Subjects Review Board of the University of Florence. Experiments involving animals have been reported according to ARRIVE guidelines (McGrath and Lilley, 2015). All efforts were made to minimize animal suffering and to reduce the number of animals used.

3.2 *In vivo* oxaliplatin model

Rats were treated with 2.4 mg kg^{-1}, oxaliplatin (Sequoia Research Products, Pangbourne, UK), administered *i.p.* for 5 consecutive days every week for 2 weeks (10 *i.p*. injections). Oxaliplatin was dissolved in a 5% glucose-water solution. The model used for the present research is consistent with the clinical practice (Di Cesare Mannelli et al., 2015b).

3.3 *Ex vivo* immunofluorescent staining

After 14 days of treatment with oxaliplatin (2.4 mg kg^{-1}, *i.p.*), rats were sacrificed; the L4/L5 segments of the spinal cord were exposed from the lumbovertebral column via laminectomy and identified by tracing the dorsal

roots from their respective DRG. Formalin-fixed cryostat sections (10 μm) were washed 3 × phosphate-buffered saline (PBS), 0.3% Triton X-100 for 5 min and then were incubated, at room temperature, for 1 h in blocking solution (PBS, 0.3% Triton X-100, 5% albumin bovine serum; PBST). Slices were incubated overnight at 4°C in PBST containing rabbit primary antisera. The primary antibody used was directed against glial fibrillary acidic protein (GFAP; rabbit, 1:1000; DAKO, Carpinteria, CA, USA) for astrocyte staining; The following day, slides were washed 3 × PBS, 0.3% Triton X-100 for 5 min and then sections were incubated in goat anti-rabbit IgG secondary antibody labeled with Alexa Fluor 568 (1:500; Invitrogen, Carlsbad, USA) and DAPI (4',6-diamidin-2-fenilindhol; 1:2000; Life Technologies-Thermo scientific, Rockford, IL, USA), a nuclei marker, in PBST at room temperature for 2 h, in the dark. For IgG staining, slices were incubated overnight at 4°C in PBST containing IgG-488 conjugated antibody (Goat anti-Rat IgG (H+L) Secondary Antibody (Alexa Fluor 488 conjugate; 1:250; Invitrogen, Carlsbad, USA). After 3 × PBS 0.3% Triton X-100 wash for 10 min, slices were mounted using ProLong Gold (Life Technologies-Thermo scientific, Rockford, IL, USA) as a mounting medium.

Negative control sections (no exposure to the primary antisera) were processed concurrently with the other sections for all immunohistochemical studies, in order to exclude the presence of non-specific immunofluorescent staining or cross-immunostaining. Fluorescent signals were detected at 200x or 400x total magnification (five microscopic fields for each experimental point) with a motorized Leica DM6000B microscope equipped with a DFC350FX.

3.4 *In vivo* permeability

Mice were treated with oxaliplatin (2.4 mg kg^{-1}, *i.p.*) for 14 days. 10 kDa texas red dextran (Invitrogen, Merelbeke, Belgium) was injected on days 1, 7 and 14 (100 mg kg^{-1}, *i.v.*) in different animal groups. After 15 min, animals were transcardially perfused and sacrificed. Prefrontal cortex, S1 and lumbar spinal cord regions were dissected and prepared for the fluorescent analysis. After dissection, different CNS regions were weighed and formamide was added (8 ml of formamide to 1 g of wet tissue weight). After that, tissues were minced

and incubated overnight at 37°C. The following day samples were centrifuged for 15 min at 15000g. 100 µl of the supernatant were used for the fluorescent analysis.

3.5 Cell line

The rat brain endothelial cell line RBE4 (Roux and Couraud, 2005; Tabbì et al., 2015) was kindly provided by Dr Vincenzo Giuseppe Nicoletti (Department of Biomedical Sciences, University of Catania, Italy). Cells (up to passage 20) were grown and maintained in alpha-minimal essential medium (alpha-MEM)/Ham's F10 (1:1) supplemented with 10% fetal bovine serum (FBS), 1% penicillin/streptomycin, 2 mM L-glutamine (EuroClone, Milano, Italy) and 1 ng/ml basic fibroblast growth factor (bFGF) (Thermo Fisher Scientific, Milano, Italy) at 37°C, 5% CO_2 in humidified atmosphere. The growth medium was routinely changed 2-3 times per week. For each experimental set-up, the cells were seeded on appropriate support for 24 h in complete growth medium. The day of the stimulation, the complete growth medium was completely changed with starvation medium (without FBS and without bFGF) adding appropriate stimuli at different concentration.

3.6 MTT assay

Cell viability was evaluated by the reduction of 3-(4,5-di- methylthiozol-2-yl)-2,5-diphenyltetrazolium bromide (MTT) by mitochondrial dehydrogenase, which directly reflects the activity of mitochondria, an indirect measurement of cell viability. RBE4 cells were plated into 96-well plates, at the density of $2.5x10^4$ cells/well, in their appropriate complete growth medium. The following day, the cells were starved as described above and treated with different concentrations of oxaliplatin (1-3-10-30-100 µM), for 8, 16 and 24 h. After treatment, the starvation medium containing stimuli was removed and substituted with 1 mg/mL MTT (in starvation medium without phenol red). The chromogenic solution was incubated for at least 20 min at 37 °C. After incubation, the formazan crystals were dissolved in 50 µl of dimethyl sulfoxide (DMSO). The absorbance was measured at 580 nm by a spectrophotometer (MultiskanFC™ microplate photometer, ThermoFisher Scientific, Milan, Italy). Each experimental point was performed in quintuplicate, for three times.

3.7 Western blotting

RBE4 cells, at the density of $3.5x10^6$ cells, were plated in Petri dishes in their appropriate complete growth medium. After 24 h the cells were serum starved and stimulated with oxaliplatin 10-30 μM, for 8, 16, and 24 h. After treatments, the medium was removed and cells were scraped in cold PBS. The cell suspensions were centrifuged at room temperature (RT) for 10 min at 1000 rpm. The pellets obtained were treated with Mem-PER™ Plus Membrane Protein Extraction Kit following the manufacture instruction, to obtain the fractionation of membrane and cytoplasm proteins. The supernatants collected were used to evaluate the protein concentration by Bradford method (Bradford, 1976). Equal amounts of protein (15 μg) were separated on a 12% polyacrylamide gel by electrophoreses and transferred onto nitrocellulose membrane (Porablot NPC, MACHEREY-NAGEL, Carlo Erba Reagents, Milano, Italy). After 1 h blocking with 3% bovine serum albumin (BSA) in Tris-buffered saline containing 0.1% Tween 20 (Tween-TBS) at RT, the blot was incubated overnight at 4°C with the rabbit primary antibody for 78 kDa glucose-regulated protein (GRP78) (ThermoFisher Scientific, Milan, Italy), cleaved caspase-3 (Cell Signalling, Leiden, Netherlands) and BAX (Santa Cruz Biotechnology, Santa Cruz, CA, USA) respectively at 1:500, 1:1000 and 1:300 final dilution in Tween-TBS/3% BSA. After washing with Tween-TBS, the goat anti-rabbit HRP secondary antibodies (Santa Cruz Biotechnology, Santa Cruz, CA, USA) was added at 1:5000 dilution in Tween-TBS for 1 h at RT, and washed again. The BAX protein was detected with the Amersham ECL Plus Western Blotting Detection Reagent (GE Healthcare, EuroClone, Milan, Italy). Protein expression levels were then quantified by image analysis software (ImageJ, National Institute of Health, USA, http://imagej.nih.gov/ij, 1.47t). β-actin normalization was performed for each sample. Each experiment was performed three times, in triplicate.

3.8 *In vitro* immunofluorescent staining

RBE4 cells were seeded on sterilized cover slips (lodged in a 6 multi-well plate) in the number of $1.5x10^5$ cells, in their appropriate complete growth medium. After 24 h the cells were serum starved and stimulated with

oxaliplatin 10-30 μM, for 8, 16, and 24 h. For shorter treatments RBE4 were seeded ($1.5x10^5$ cells) on sterilized cover slips (lodged in a 6 multi-well plate), in their appropriate complete growth medium After 24 h cells were treated with oxaliplatin (10-30 μM) for 10 min. After treatments, the medium was removed and each cover slip was washed twice with cold PBS followed by fixation with paraformaldehyde 3.7% in PBS for 10 min. at RT. After fixation, two more washes with cold PBS were performed; the cover slips were dried at RT for at least 1 h.

The fixed cells where rinsed in cold PBS for three times and, only for ZO1 evaluation, the antigen retrieval was performed for 10 min in 95°C solution with 5% urea in pH 9.5 Tris 100 mM. Then, cells were permeabilized with a 1% solution of TRITON X-100 in PBS for 10 min at RT. Following, cells were washed three times with PBS and then incubated for 15 min in a blocking solution (1% albumin bovine serum (BSA) in PBS) at RT. Each cover slip was incubated overnight at 4°C with the rabbit primary antibody anti-ZO1 (1:100) and with Alexa-488-conjugated phalloidin (1:200; ThermoFisher Scientific, Milan, Italy), in 1% BSA. The day after, cells were washed three times with PBS and each cover slip was incubated in goat anti-rabbit (for ZO1) immunoglobulin G (IgG) secondary antibody, conjugated with Alexa Fluor 488 (far red) (1:200; Invitrogen, Milan, Italy) for 1 h at RT. After that, two washes were performed with PBS and DAPI (4',6-diamidin-2-fenilindhol; 1:2000 dilution; Invitrogen, Milan, Italy) was added for 5 min at RT to each cover slip. Eventually, cover slip glasses were mounted using Fluoromount anti-fade solution (ThermoFisher Scientific, Milan, Italy) on cover slides. Fluorescent signals were detected at 20x or 40x total magnification (five microscopic fields for each experimental point) with a motorized Leica DM6000B microscope equipped with a DFC350FX. Fifteen pictures from each field were captured. The experiments were performed three times.

3.9 Caspase-3 enzimatic activity

RBE4 cells were plated in 6-well plates ($5x10^5$/well) in appropriate complete growth medium. The following day, cells were starved and stimulated with oxaliplatin 10-30 μM for 8, 16, and 24 h. After treatment, cells were scraped in 100 mM lysis buffer (200 mM Tris–HCl buffer, pH 7.5, containing 2 M NaCl,

20 mM EDTA, and 0.2% Triton X-100). Fifty microliters of the supernatants were incubated with 25 μM fluorogenic peptide caspase-3 substrate rhodamine 110 bis-(N-CBZ-L-aspartyl-L-glutamyl-L-va- lyl-L-aspartic acid amide) (Z-DEVD-R110; Molecular Probes) at 25 °C for 30 min. The amount of cleaved substrate in each sample was measured in a 96-well plate fluorescent spectrometer (Perkin-Elmer; excitation at 496 nm and emission at 520 nm). Each experiment was performed two times, in duplicate.

3.10 Extracellular ATP quantification

RBE4 cells were plated in 6-well plates ($5x10^5$/well) in appropriate complete growth medium. The following day, cells were starved and stimulated with oxaliplatin (10-30 μM) for 8, 16, and 24 h. For shorter treatments, RBE4 cells were plated in 6-well plates ($5x10^5$/well) and growth till the confluence. Then cells were treated with oxaliplatin (10-30 μM) for 10 min in the presence or in the absence of inhibitors. After treatments, the mediums were harvested and 50μl were processed following the manufacture's procedure (ATPlite - Luminiscence ATP Detection Assay System, PerkinElmer Italia, Milan, Italy). The extracellular ATP was quantified using a 96-well plate luminescence reader (Perkin-Elmer). Each experiment was performed two times, in duplicate.

3.11 Calcium imaging

RBE4 cells were seeded onto 9.2 cm2 petri dishes (TPP, Novolab, Geraardsbergen, Belgium) and experiments were performed at confluence. After 8 or 16 h treatment with oxaliplatin 10 or 30 μM, RBE4 monolayers were loaded with a mixture of 10 μmol/L fluo3-AM, 1 mmol/L probenecid, and 0.01% pluronic acid in HBSS-Hepes (in mmol/L: 0.95 CaCl2; 0.81 MgSO4; 13 NaCl; 0.18 Na2HPO4; 5.36 KCl; 0.44 KH2PO4; 5.55 D-glucose; and 25 Hepes; standard solution for Ca^{2+} experiments) during 1 h at RT. After that, petri dishes (RBE4) were washed and cells were left for an additional 15 min at RT in HBSS-Hepes/probenecid to allow for de-esterification. For Ca^{2+} free experiments 4.4 mM of EGTA as Ca^{2+} chelator was added to the Ca^{2+} standard solution. Cells were thereafter transferred to an inverted

epifluorescence microscope (Eclipse TE 300, Nikon Belux, Brussels, Belgium). Solutions were gently added to petri dishes before acquiring images. Images were taken every second with a 40X oil immersion objective (NA 0.8) and an electron multiplying CCD camera (Quantem 512SC; Photometrics, Tucson, AZ, USA). We used a Lambda DG-4 filterswitch (Sutter Instrument Company, Novato, CA, USA) to deliver excitation at 482nm and captured emitted light via a 505-nm long-pass dichroic mirror and a 535-nm bandpass filter (35 nm bandwidth). Recordings and analysis were performed with custom-developed QuantEMframes and Fluoframes software written in Microsoft Visual C+ + 6.0. Ca^{2+} changes triggered by ATP (1 μM) or direct application of oxaliplatin (10 or 30 μM) were recorded over a 10-minute observation period. Several pharmacological substances were used to further investigate the nature of the recorded Ca^{2+} responses, including the phospholipase C (PLC) inhibitor U-73122 (10 μM; Carbosinth, Compton - Berkshire - RG20 6NE - UK), the $InsP_3$ receptor (Ins3PR) inhibitor Xestospongin C (5 μM; Carbosinth, Compton - Berkshire - RG20 6NE - UK) and the Panx-1 channel blocker ^{10}Panx1 (100 μM; ProteoGenix, Schiltigheim - France). Analysis of the Ca^{2+} responses was done by calculating the relative fluorescence change of the Ca^{2+} reporter dye DF/F_0 ($F-F_0/F_0$) and calculating the area under the curve (AUC) of the DF/F_0 response over the 10 min recording period after application of the trigger condition. The AUC values given represent AUC divided by 600, which are the number of datapoints in the 10 min recording window.

3.12 Statistical analysis

Results were expressed as means ± S.E.M. and the analysis of variance was performed by analysis of variance. A Bonferroni's significant difference procedure was used as post hoc comparison. P values of less than 0.05 or 0.01 were considered significant. Data were analyzed using the ''Origin 8.1'' software.

4. Results

4.1 *Ex vivo* analysis

Immonuglubulin G (IgG) staining of the rats' lumbar spinal cord daily treated with oxaliplatin (2.4 mg kg^{-1}, *i.p.*) for 14 days was performed to evaluate BSCB opening (Fig. 1). As shown in Fig. 1, on day 14, IgG extravasation was found in the lumbar spinal cord parenchyma of oxaliplatin-treated rats.

Moreover, rat spinal cord slices were immuno-labeled with GFAP (yellow, for astrocytes) and RECA-1 (red, for endothelial cells). As depicted in Fig. 2, in control animals GFAP-positive cells showed typical non-reactive astrocyte morphology, while in the oxaliplatin-treated group several astrocytes were reactive displaying hypertrophy and increased cell density. To note, astrocyte reactivity was found particularly increased around blood vessels (Fig. 2).

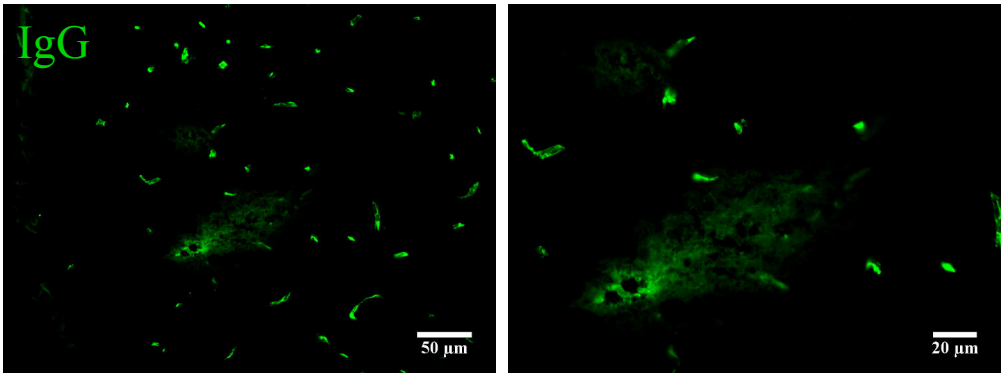

Figure 1. *Ex vivo* analysis. ImmunoglobulinG extravasation in the lumbar spinal cord parenchyma after oxaliplatin chronic treatment. Representative images of IgG-Alexafluor 488 conjugated in a lumbar spinal cord section of rat treated with oxaliplatin 2.4 mg kg^{-1} (*i.p.*) for 14 days. Digitalized images were collected (five microscopic fields for each experimental point) by a motorized Leica DM6000B microscope equipped with a DFC350FX. Representative images of 20X and 40X magnification of lumbar spinal cord section.

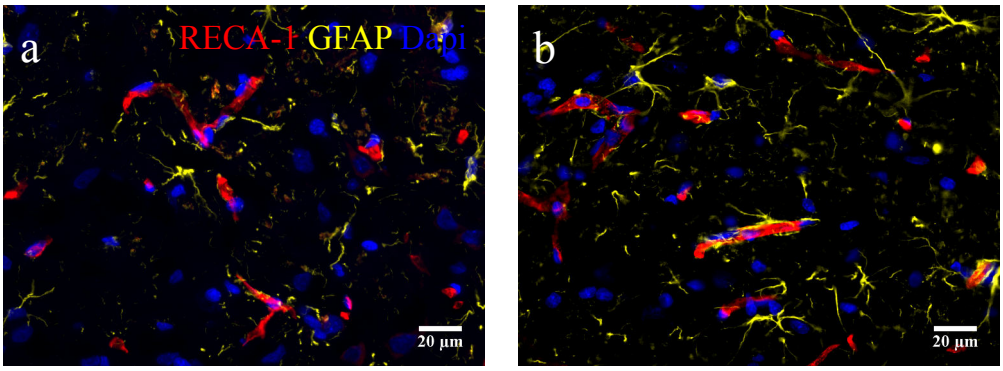

Figure 2. *Ex vivo* analysis. The NeuroVascular Unit in the lumbar spinal cord after oxaliplatin chronic treatment. Representative images of merged RECA-1-labelled endothelial cells (red), GFAP-labelled astrocyte cells (yellow), plus DAPI-labelled cell nuclei (blue) of lumbar spinal cord section of (a) vehicle-treated rats or (b) rats treated with oxaliplatin 2.4 mg kg^{-1} (*i.p.*) for 14 days. Digitalized images were collected (five microscopic fields for each experimental point) by a motorized Leica DM6000B microscope equipped with a DFC350FX. Representative images of 40X magnification of lumbar spinal cord section.

4.2 *In vivo* permeability

The possibility to induce changes in the BBB or in the BSCB permeability by oxaliplatin was investigated *in vivo* in specific brain and spinal cord areas. Mice were injected with oxaliplatin (2.4 mg kg^{-1}, *i.p.*) for 14 days. On day 1, 7 and 14 different groups of animals were injected with 10 kDa dextran texas red (100 mg kg^{-1}, *i.v.*) as a marker for endothelial permeability. After 15 min animals were sacrificed and prefrontal cortex, somatosensory S1, and lumbar spinal cord areas were explanted in order to evaluate the inner fluorescence. As depicted in Fig. 3, after 7 days of treatment, oxaliplatin significantly increased the permeability of both BBB and BSCB, precisely in prefrontal cortex (176.22 ± 9.6% oxaliplatin, day 7 vs. 100.0 ± 18.0% control, day 7) and lumbar spinal cord regions (190.4 ± 22.0% oxaliplatin, day 7 vs. 100.0 ± 12.7% control, day 7) (Fig. 3).

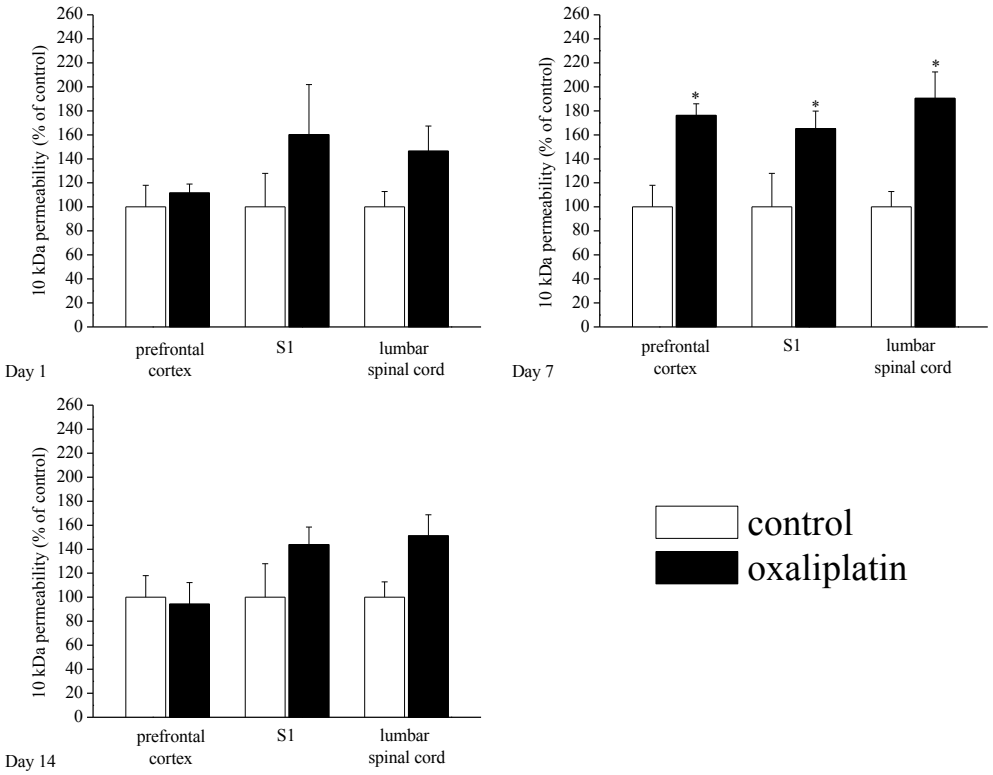

Figure 3. Effect of oxaliplatin on *in vivo* BBB/BSCB permeability. Mice were treated with oxaliplatin for 14 days (2.4 mg kg^{-1}, *i.p.*) for 14 days. 10 kDa dextran texas red was injected on days 1, 7 and 14 (100 mg kg^{-1}, *i.v.*) in different animal groups. After 15 min animals were transcardially perfused and sacrificed. Prefrontal cortex, S1 and lumbar spinal cord regions were dissected and their fluorescence was determined. All the results are expressed as the mean ± S.E.M of six animals per group performed in two experimental sets. *P<0.05 vs. control.

4.3 MTT assay

The MTT assay was performed, to evaluate RBE4 viability after oxaliplatin treatment for 8, 16, and 24 h at different concentrations (1, 3, 10, 30 and 100 µM). The anticancer compound affected cell vitality in a dose-dependent and time-dependent manner. As depicted in Fig. 4, cell viability was significantly decreased after treatment with 100 µM of oxaliplatin for 8 h (83.0 ± 2.6%, oxaliplatin 100 µM, 8 h). Otherwise, prolonged exposure to the antineoplastic agent significantly impaired cell vitality starting from 10 µM, after 16 h (83.0 ± 1.9%, oxaliplatin 10 µM, 16 h), and 3 µM, after 24h (78.0 ± 1.8%,

oxaliplatin 3 μM, 24 h), respectively (Fig. 4).

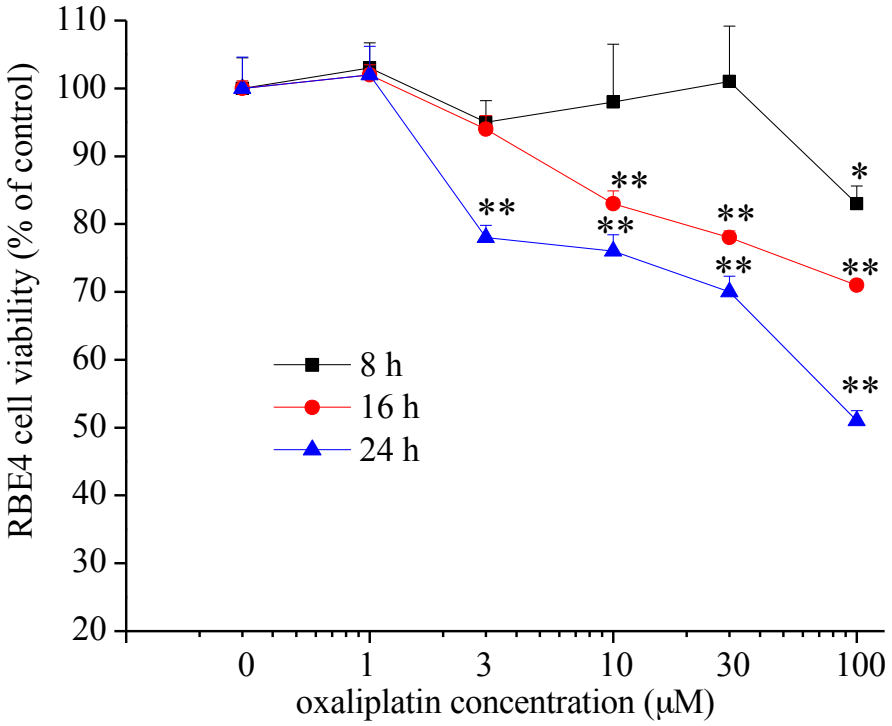

Figure 4. Effect of oxaliplatin on RBE4 cell viability. RBE4 ($2.5x10^4$ cells/well) viability was quantified by MTT assay after incubation with oxaliplatin (1-100 μM) for 8, 16 or 24 h. Absorbance was measured at 580 nm. Values were expressed in percentage of control absorbance as the mean ± S.E.M of three experiments. Control condition was arbitrary set at 100%. *P<0.05 and **P<0.01 vs. control.

4.4 ER stress - GRP78 expression

The effect of oxaliplatin on the ER stress was evaluated via the measurement of GRP78 levels (Fig. 5). The histogram indicates that GRP78 levels significantly increased after 8 h treatment with oxaliplatin at the dose of 10 and 30 μM. On the other hand, only oxaliplatin 30 μM augmented GRP78 expression after 24 h (Fig. 5).

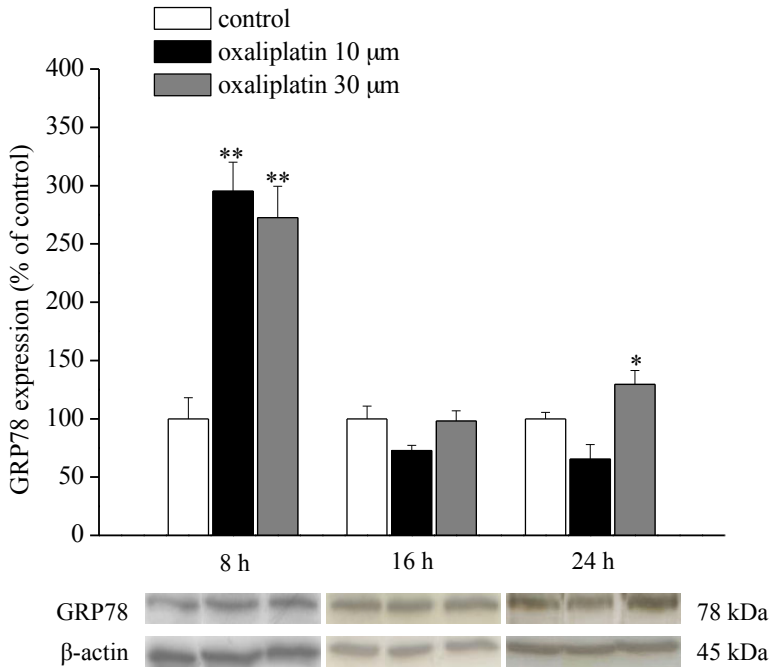

Figure 5. ER-stress marker GRP78 protein expression levels in RBE4 cells. RBE4 cells ($3.5x10^6$ cells/Petri dish) were exposed to oxaliplatin (10-30 μM) for 8, 16 or 24 h. Western blot analysis was performed on cell homogenates, using a specific antibody for GRP78 (78 kDa). Representative immunoblot and densitometric analysis are shown. Densitometric analysis of western blot was performed by ImageJ software. Data are expressed as percentage of control. β-actin normalization was performed for each sample. *P<0.05 and **P<0.01 vs. control.

4.5 Ca^{2+} imaging - prolonged exposure to oxaliplatin

The effect on $[Ca^{2+}]_i$ after exposure of RBE4 cells to oxaliplatin is depicted in Fig. 6. Changes of $[Ca^{2+}]_i$ were expressed as area under the curve (AUC) over a 10 min recording window. Following treatment with oxaliplatin (10 or 30 μM) for 8 or 16 h, RBE4 cells were stimulated with ATP 1 μM which activates various purinergic receptors including P2X and P2Y receptors (De Bock et al., 2013). In the RBE4 exposed to 10 or 30 μM oxaliplatin for 16 h, the ATP stimulation caused a smaller Ca^{2+} response compared to the control condition (Fig. 6). Of note, the effect of the lower concentration of oxaliplatin amounted

to 3.7 ± 0.3 AUC, for 10 μM and 3.9 ± 0.1 AUC, for 30 μM vs. 6.0 ± 0.7 AUC for control measurements. In the 8 h oxaliplatin condition, no significant changes of $[Ca^{2+}]_i$ were detected in comparison to control conditions (Fig. 6a).

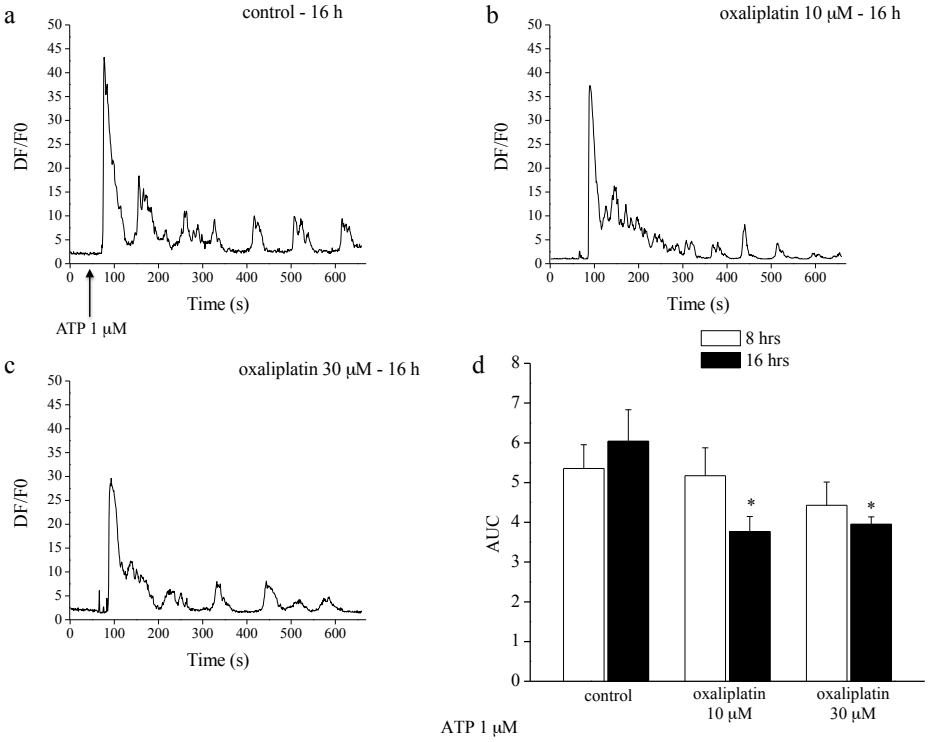

Figure 6. Effect of oxaliplatin on in the $[Ca^{2+}]_i$ - prolonged treatment. ATP stimulation. Typical example traces of $[Ca^{2+}]_i$ changes in selected RBE4 cells, pre-treated with or without oxaliplatin 10 or 30 μM for 16 h, and triggered with ATP (1 μM) (a, b, c). $[Ca^{2+}]_i$ changes showed an initial peak followed by ongoing oscillatory changes. (d) demonstrates summary data of the area under the $[Ca^{2+}]_i$ curve (AUC) of the various conditions shown. All the results are expressed as the mean ± S.E.M of three experiments. *P<0.05 vs. control.

The previous results may indicate the occurrence of store depletion after 16 h oxaliplatin treatment. In order to further scrutinize this, we tested the store Ca^{2+} content by applying the SERCA inhibitor thapsigargin (2 μM) under zero extracellular Ca^{2+} conditions to prevent a contribution from external Ca^{2+} entry. Thapsigargin provokes increased Ca^{2+} store leakage by inhibiting Ca^{2+} reuptake in the store; as a result, the thapsigargin-triggered Ca^{2+} transient gives an indication of the Ca^{2+} content of the store. We applied the thapsigargin protocol for RBE4 cells treated with 10 or 30 μM oxaliplatin for 16 h. As shown in Fig. 7, thapsigargin applied under zero extracellular Ca^{2+} conditions

caused an immediate increase of $[Ca^{2+}]_i$ amounting to 2.5 ± 0.0 AUC (AUC of the $[Ca^{2+}]_i$ response to thapsigargin). By contrast, cells treated with oxaliplatin exhibited less thapsigargin-induced $[Ca^{2+}]_i$ increase. The effect of oxaliplatin 10 μM was more pronounced (1.6 ± 0.1 AUC, oxaliplatin 10 μM and 2.0 ± 0.2 AUC, oxaliplatin 30 μM) (Fig. 7).

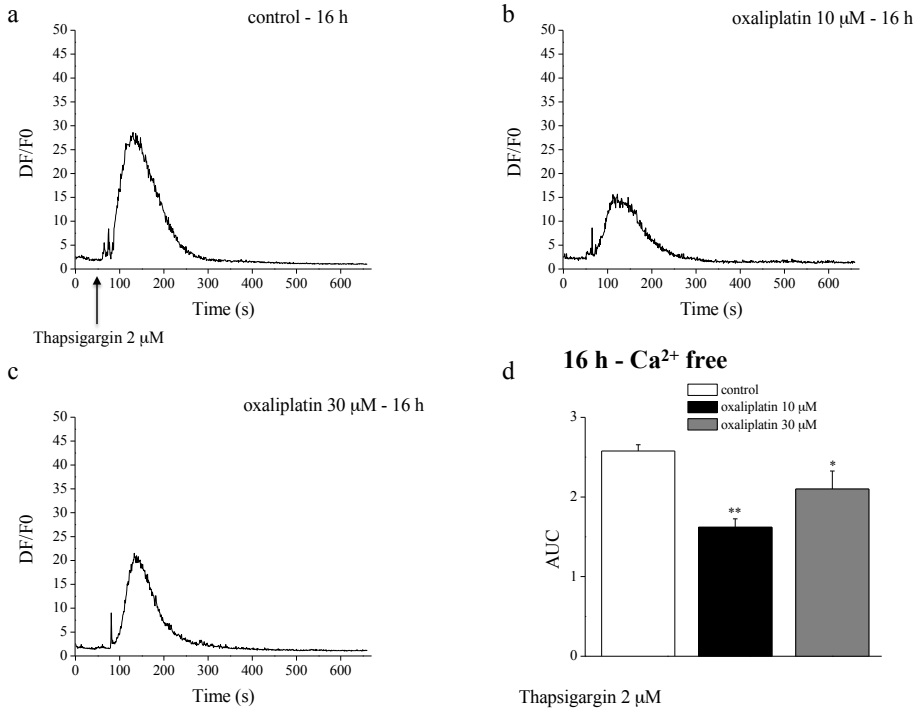

Figure 7. Effect of oxaliplatin on $[Ca^{2+}]_i$ - prolonged treatment. Thapsigargin stimulation. In the panels on the left typical example traces of $[Ca^{2+}]_i$ changes in selected RBE4 cells, pre-treated with or without oxaliplatin 10 or 30 μM for 16 h, and triggered with Thapsigargin (2 μM) (a, b, c) are shown. The switch from normal to zero extracellular Ca^{2+} condition was done just before the 1 min control recording. (d) demonstrates summary data of the area under the $[Ca^{2+}]_i$ curve (AUC) of the various conditions shown. All the results are expressed as the mean ± S.E.M of three experiments. *P<0.05 and **P<0.01 vs. control.

4.6 Caspase-3 activity and BAX expression

In order to detect changes in the metabolic and apoptotic pathways the activition of caspase-3 and the expressions of BAX were analysed.

The activity of caspase-3 was evaluated by measuring the expression of its

cleaved form. As depicted in Fig. 8, oxaliplatin both at 10 and 30 μM increased the expression of the cleaved caspase-3 after 8, 16 and 24 h treatment (Fig. 8). To validate these data, the activity of caspase-3 was measured with a fluorescence assay. Also in this case the antineoplastic agent, at the concentration of 10 and 30 μM, caused the caspase-3 activation after 8, 16 and 24 h (Fig. 9).

To investigate the effect of the anticancer agent on the apoptotic pathway, the expression of the pro-apoptotic protein BAX was analysed. The Fig.10 shows that BAX levels were slightly increased after 24 h treatment with oxaliplatin 30 μM (Fig. 10).

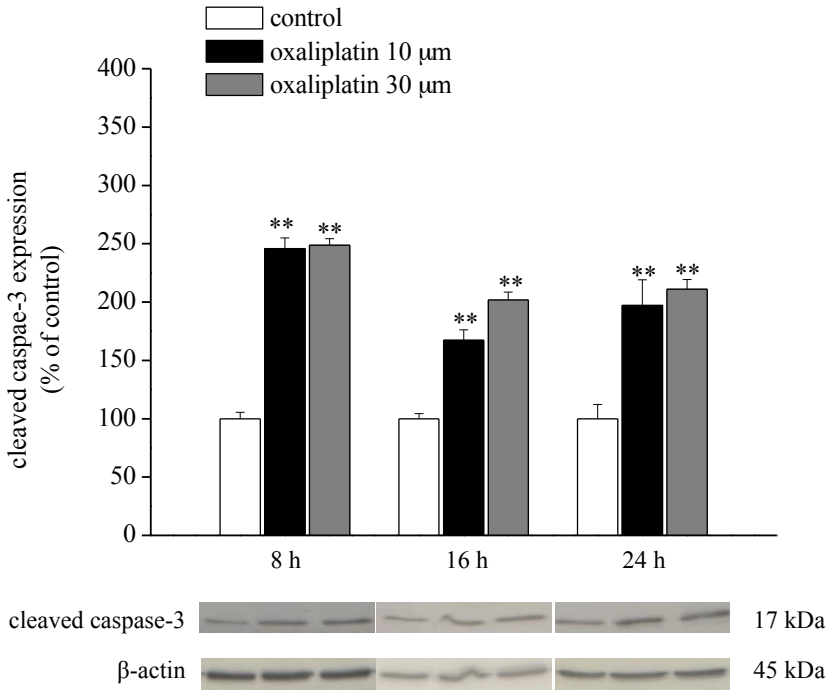

Figure 8. Cleaved caspase-3 protein expression levels in RBE4 cells. RBE4 cells ($3.5x10^6$ cells/Petri dish) were exposed to oxaliplatin (10-30 μM) for 8, 16 or 24 h. Western blot analysis was performed on cell homogenates, using a specific antibody for the cleaved form of caspase-3 (17 kDa). Representative immunoblot and densitometric analysis are shown. Densitometric analysis of western blot was performed by ImageJ software. Data are expressed as percentage of control. β-actin normalization was performed for each sample. *P<0.05 and **P<0.01 vs. control.

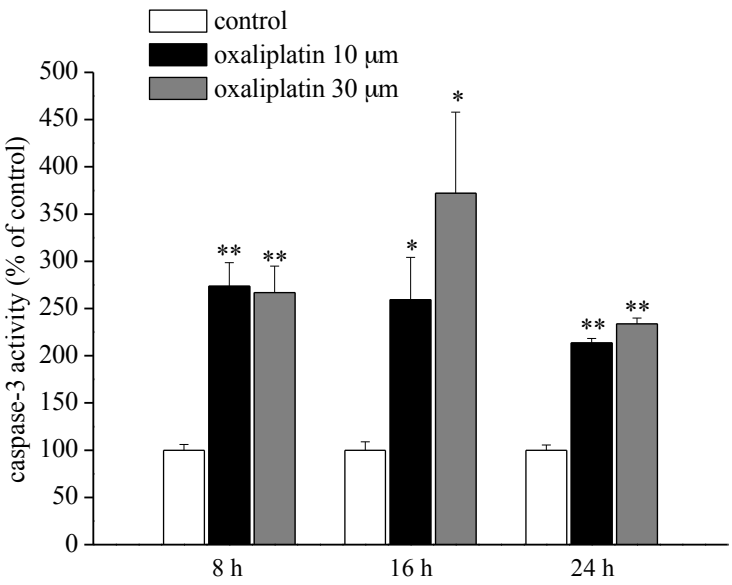

Figure 9. Caspase-3 enzimatic activity in RBE4 cells. RBE4 cells ($5x10^5$/well) were exposed to oxaliplatin (10-30 μM) for 8 or 16 or 24 h. Caspase-3 activity was measured by a fluorescence assay. Values are expressed in percentage of control (100%, untreated cells). All the results are expressed as the mean ± S.E.M of three experiments. Control condition was arbitrary set at 100%. **P<0.01 vs. control.

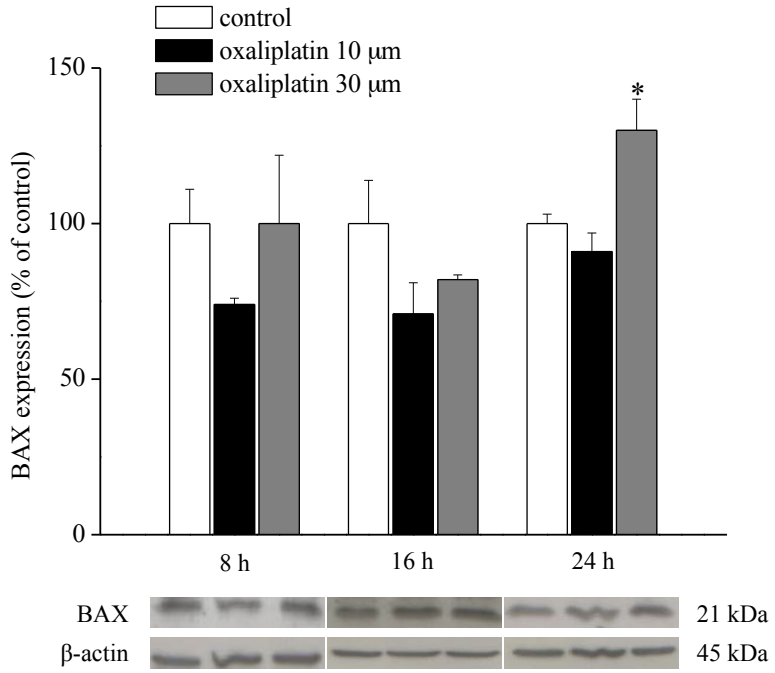

Figure 10. BAX protein expression levels in RBE4 cells. RBE4 cells ($3.5x10^6$ cells/Petri dish) were exposed to oxaliplatin (10-30 μM) for 8, 16 or 24 h. Western blot analysis was performed on cell homogenates, using a specific antibody for BAX (21 kDa). Representative immunoblot and densitometric analysis are shown. Densitometric analysis of western blot was performed by ImageJ software. Data are expressed as percentage of control. β-actin normalization was performed for each sample. *P<0.05 vs. control.

4.7 Cytochrome C release from mitochondria

The release of the cytochrome C from mitochondria was analysed by immunofluorescent staining (Fig. 11). As shown in Fig. 11, oxaliplatin treatment did not cause cytochrome C release in the cytosolic compartment after neither 8 h nor 16 h, indicating the absence of mitochondrion impairment.

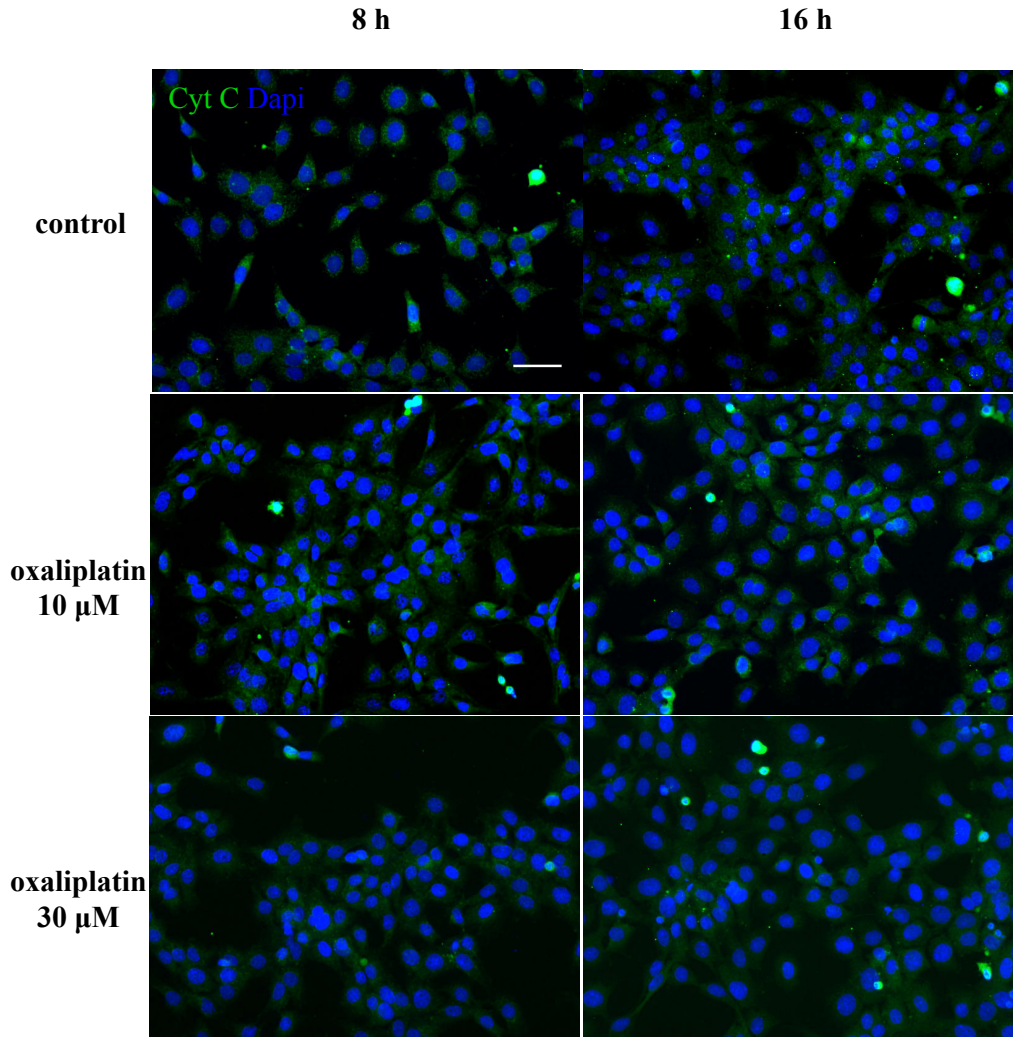

Figure 11. Mitochondrial release of cytochrome C. RBE4 cells ($1.5x10^5$ cells/cover slip) were exposed to oxaliplatin (10-30 µM) for 8 h or 16 h. Cytochrome C was detetected by immunofluorescent staining. Digitalized images were collected (five microscopic fields for each experimental point) by a motorized Leica DM6000B microscope equipped with a DFC350FX. Each experimental point was performed in triplicate, for three different set of experiments. Total magnification: 20X. Scale bar: 50 µm.

4.8 ATP release - prolonged exposure to oxaliplatin

The evaluation of the ATP concentration released from RBE4 after treatment with oxaliplatin is shown in Fig. 12. The antineoplastic compound, at the dose of 10 µM augmented the exit of ATP form RBE4 after 8 h treatment (144.7 ± 8.0%, oxaliplatin 10 µM vs. 100.0 ± 2.4%, control). Otherwise, the higher concentration of oxaliplatin (30 µM) doubled the extracellular ATP if

compared with the control condition after 8 h but poorly increased the exit of nucleotide after 16 h treatment. Moreover, an even longer treatment (24 h) with 30 μM of oxaliplatin dramatically elevated the quantity of extracellular ATP (val ± val %, oxaliplatin 10 μM versus 100.0 ± 15.9%, control) (Fig. 12).

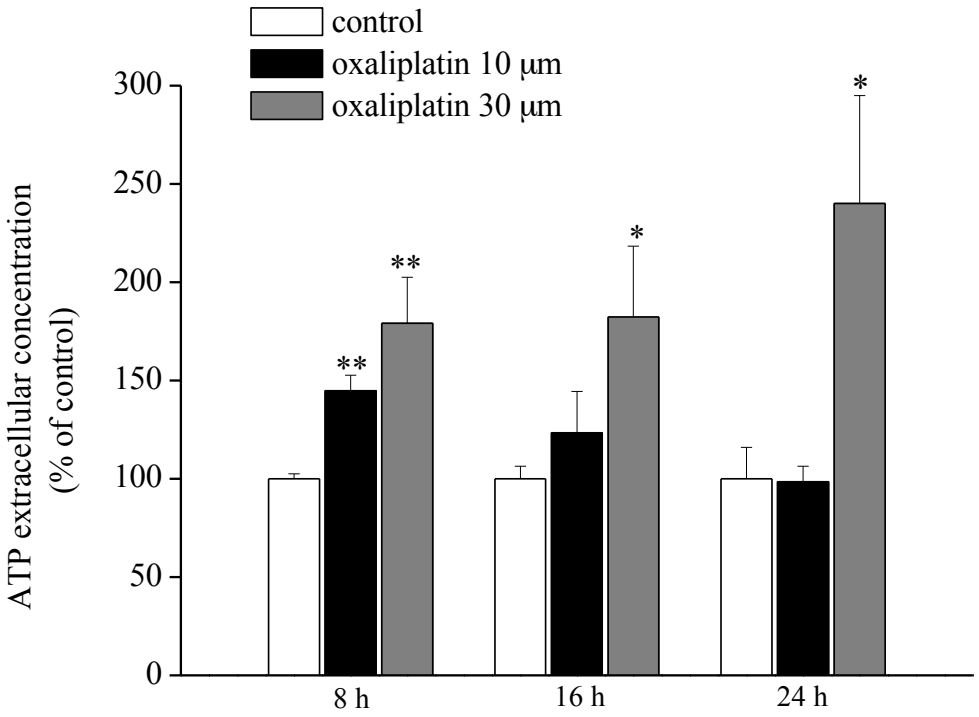

Figure 12. Extracellular ATP release - prolonged treatment with oxaliplatin. RBE4 (5 x 10^5/well) were treated with oxaliplatin (10 or 30 μM) for 8, 16, or 24 h. Extracellular ATP concentration in the medium was measured by luminescence assay. All the results are expressed as the mean ± S.E.M of three experiments. Control condition was arbitrary set at 100%. *P<0.05 vs. control.

4.9 TJs and cytoskeleton distribution - prolonged exposure to oxaliplatin

To investigate the assessment of TJ complex, the localization of ZO-1 and the cytoskeleton protein F-actin were detected with immunofluorescence staining. As shown in Fig. 13, in control condition, ZO-1 is localized contiguously at the cell-cell edges accordingly to its sealing function. On the other hand, ZO-1 distribution became patchy and significantly discontinuous in RBE4 cells treated with oxaliplatin both at increasing concentrations and times, thus indicating a breakdown to its function integrity. The F-actin cytoskeleton is

functionally coupled to the cytoplasmic domains of TJs such as ZO-1 and its distribution is strictly implicated in the regulation of the BBB integrity (Shiu et al., 2007). The characteristic distribution in control (untreated) cells is localized on the cells' edges. This localization is lost by oxaliplatin treatment in a dose- and time-dependent manner. To note, actin filaments migrates to the perinuclear region in a dose- and time-dependent manner (Fig. 14).

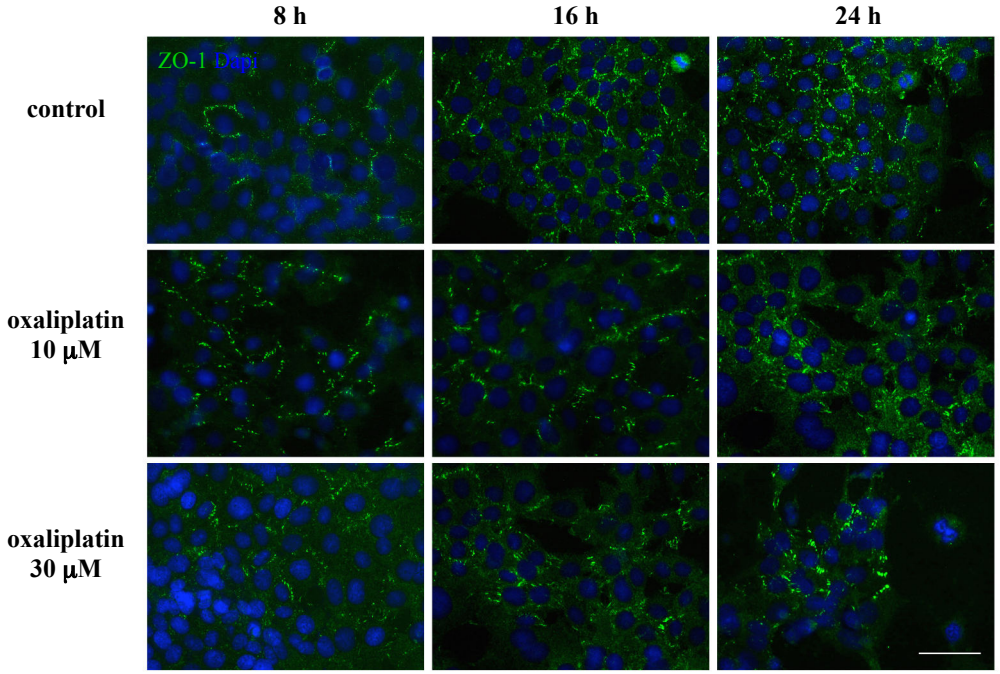

Figure 13. Effect of oxaliplatin on ZO-1 distribution - prolonged treatment. RBE4 cells ($1.5x10^5$ cells/cover slip) were exposed to oxaliplatin (10-30 μM) for 8, 16 or 24 h. ZO-1 protein was detetected by immunofluorescent staining. Digitalized images were collected (five microscopic fields for each experimental point) by a motorized Leica DM6000B microscope equipped with a DFC350FX. Each experimental point was performed in triplicate, for three different set of experiments. Total magnification: 20X. Scale bar: 50 μm.

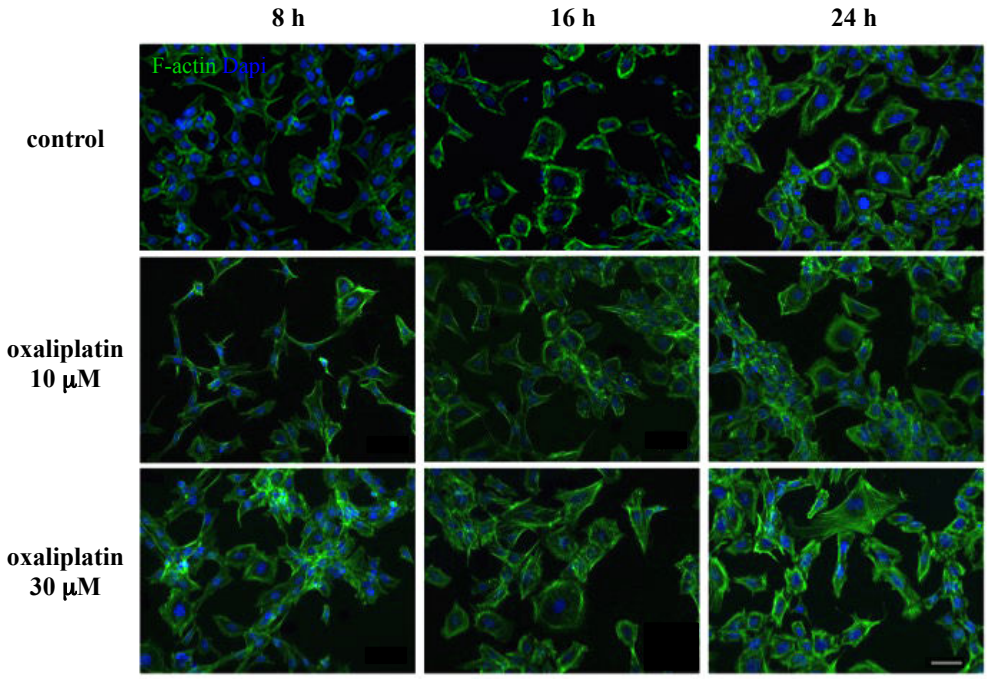

Figure 14. Effects of oxaliplatin on F-actin distribution - prolonged treatment. RBE4 cells ($1.5x10^5$ cells/cover slip) were exposed to oxaliplatin (10-30 µM) for 8, 16 or 24 h. F-actin protein was detected by immunofluorescent staining. Digitalized images were collected (five microscopic fields for each experimental point) by a motorized Leica DM6000B microscope equipped with a DFC350FX. Each experimental point was performed in triplicate, for three different set of experiments. Total magnification: 20X. Scale bar: 20 µm.

4.10 Ca^{2+} imaging - acute effects of oxaliplatin

The $[Ca^{2+}]_i$ was measured even after exposure of $[Ca^{2+}]_i$ responses were also measured in RBE4 cells in response to acute application of oxaliplatin at the doses of 10 and 30 µM and applied for 10 min. In this case, the higher dose of oxaliplatin significantly increased the $[Ca^{2+}]_i$ with respect to the control condition (5.4 ± 0.3 AUC, oxa 30 µM vs. 1.8 ± 0.3 AUC, control) (Fig. 15a). This response was partially blocked in the presence of the phospholipase C (PLC) inhibitor U-73122 (10 µM, added together with OR before oxaliplatin ???) and the InsP3R inhibitor Xestospongin C, at the dose of 5 µM (3.3 ± 0.0 AUC, oxa 30 µM + U-73122 10 µM and 3.0 ± 0.7 AUC, oxa 30 µM + Xes C 5 µM). Moreover, [10]Panx (100 µM), a peptide blocker of Panx1 channels

significantly decreased the oscillations triggered by oxaliplatin (2.6 + 0.6 AUC, oxa 30 μM + ^{10}Panx 100 μM) (Fig. 15a). On the other hand, oxaliplatin-evoked Ca^{2+} responses were suppressed if the cells were exposed to Ca^{2+}- free extracellular conditions (Ca^{2+} ≈1 nM) (2.9 ± 0.4 AUC, oxa 30 μM vs. 2.5 ± 0.7 AUC, control) (Fig. 15b).

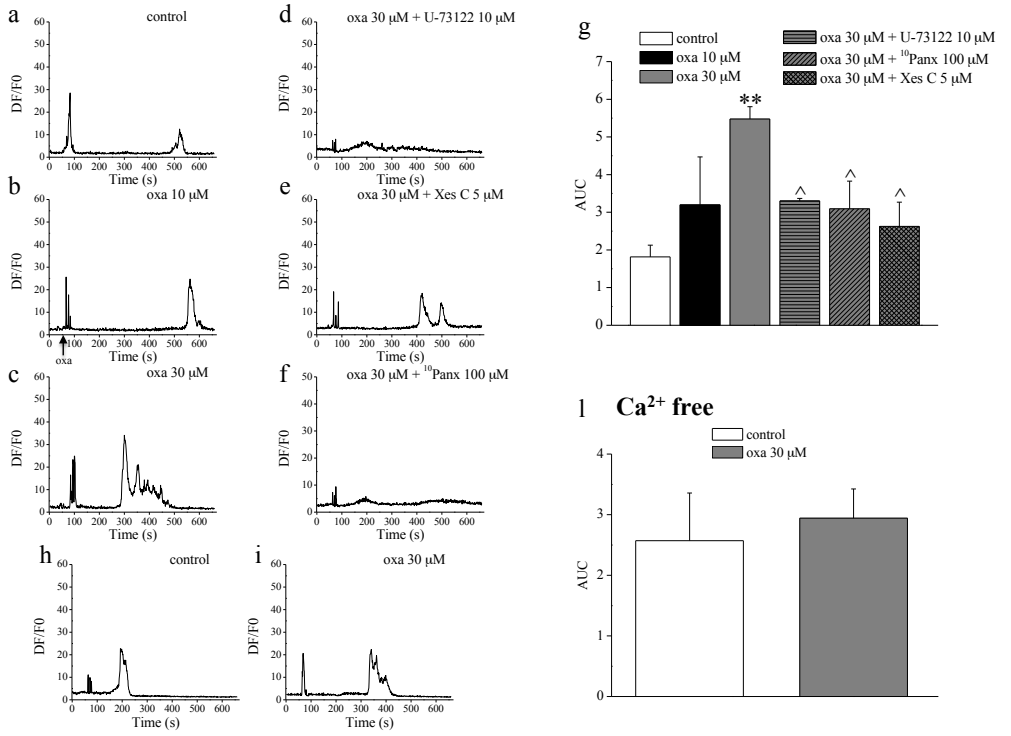

Figure 15. Acute effect of oxaliplatin on the $[Ca^{2+}]_i$ - short treatment. In the panels on the left typical traces of $[Ca^{2+}]_i$ changes in selected RBE4 cells, treated with oxaliplatin 10 or 30 μM, in the presence or in the absence of U-73122 10 μM, Xes C 5 μM, 10Panx 100 μM or in Ca^{2+}-free conditions (b, c, d, e, f, g, i, l) are shown. The switch from normal to zero extracellular Ca^{2+} condition was done just before the 1 min control recording. (g, l) demonstrate summary data of the area under the $[Ca^{2+}]_i$ curve (AUC) of the various conditions shown. All the results are expressed as the mean ± S.E.M of three experiments. *P<0.05 and **P<0.01 vs. control.

4.11 ATP release - acute effect of oxaliplatin

Short exposure to the antineoplastic agent (10 min) increased the extracellular concentration of ATP if compared to the control condition (191.5 ± 12.4% oxaliplatin 30 μM vs. 100.0 ± 9.8%, control) (Fig. 16a). Otherwise, the

treatment with oxaliplatin in Ca^{2+}- free + EGTA extracellular conditions (Ca^{2+} ≈1 nM) did not not affect the nucleotide release (92.5 + 15.0%, oxaliplatin 30 μM vs. 100.0 + 8.7%, control) (Fig. 16b).

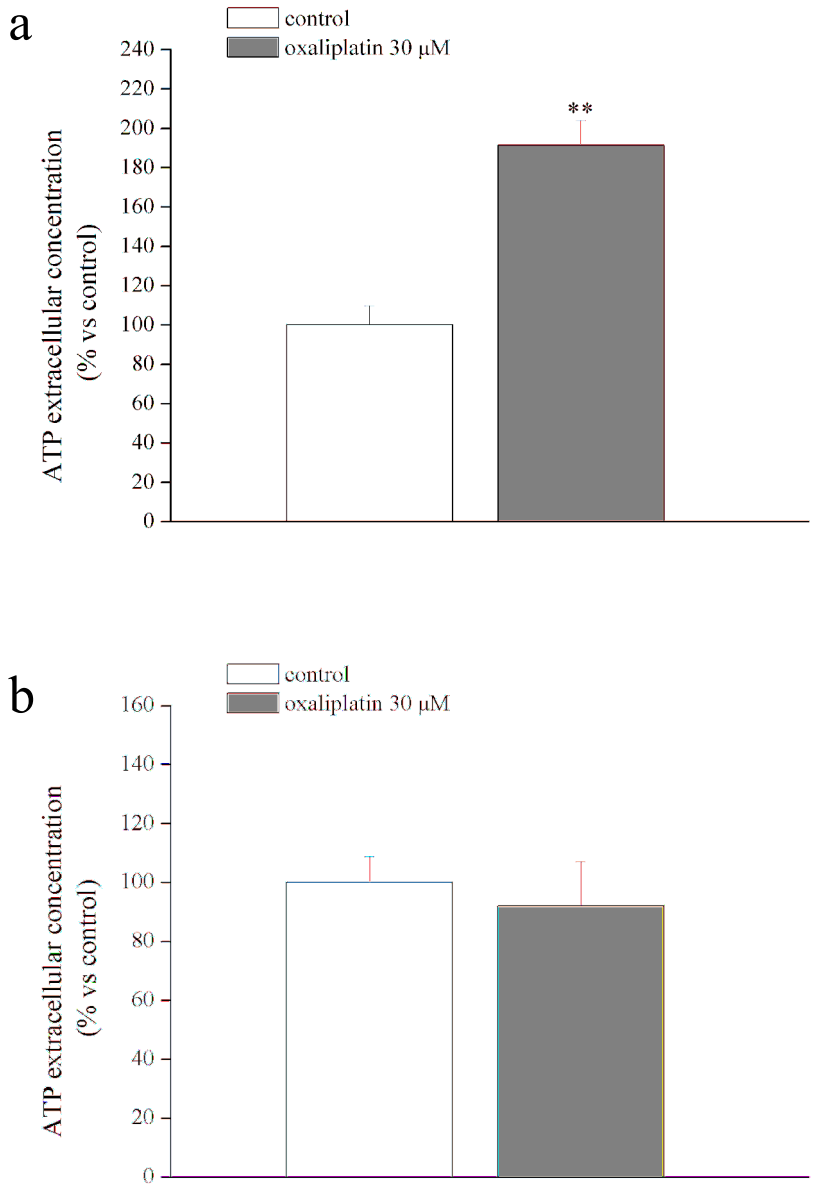

Figure 16. Extracellular ATP release - short treatment with oxaliplatin. RBE4 (5 x 10^5/well) were treated with oxaliplatin 30 μM for 10 min in the presence (a) or in the absence (b) of extracellular calcium ([Ca^{2+} ≈1 nM). Extracellular ATP concentration in the medium was measured by luminescence assay. All the results are expressed as the mean ± S.E.M of three experiments. Control condition was arbitrary set at 100%. *P<0.05 and **P<0.01 vs. control.

4.12 TJs and cytoskeleton distribution - short exposure to oxaliplatin

The localization of ZO-1 and the organization of the cytoskeletal protein F-actin were investigated in RBE4 after 10 min treatment of oxaliplatin 30 µM (Fig. 17). Even in this case, ZO-1 arrangement was altered, becoming patchy and with distinguishable discontinuation (Fig. 17a). Additionally, the correct organization of F-actin was partially lost. As shown in Fig. 17b, the treatment with oxaliplatin caused the migration of protein to the perinuclear space (Fig. 17b).

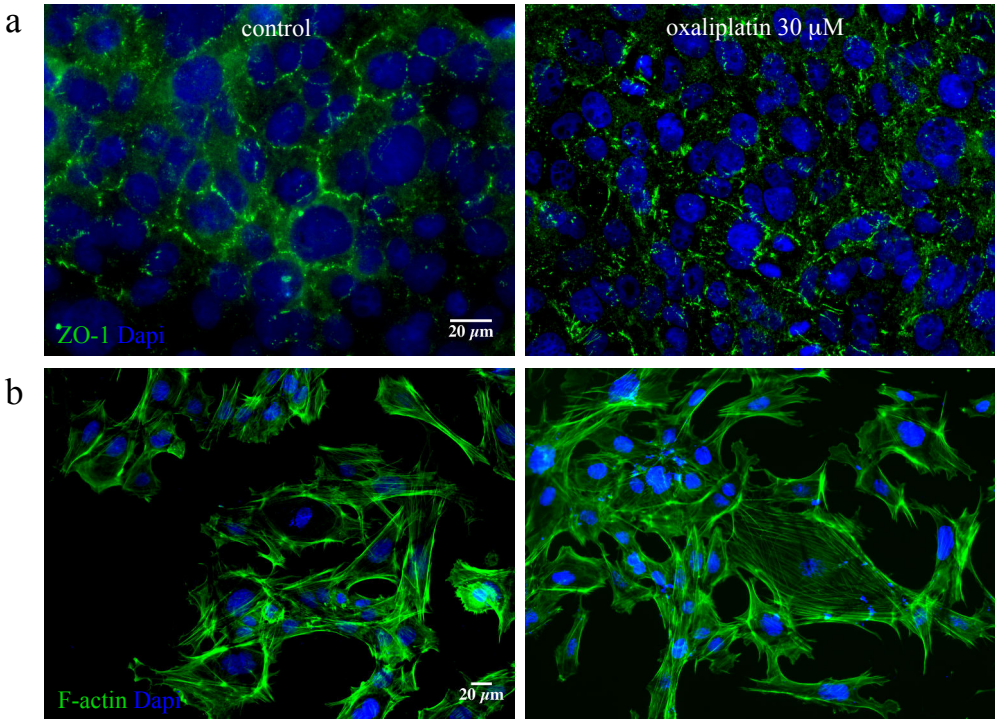

Figure 17. Effects of oxaliplatin on ZO-1 and F-actin distribution - short treatment. RBE4 cells ($1.5x10^5$ cells/cover slip) were exposed to oxaliplatin 30 µM for 10 min. ZO-1 (a) and F-actin (b) were detected by immunofluorescent staining. Digitalized images were collected (five microscopic fields for each experimental point) by a motorized Leica DM6000B microscope equipped with a DFC350FX. Each experimental point was performed in triplicate, for three different set of experiments. Total magnification: 40X. Scale bar: 20 µm.

5. Discussion

Oxaliplatin is one of the most extensively used chemotherapy agents for the treatment of the metastatic colo-rectal cancer (Lonardi et al., 2016). Although its anticancer efficacy, it provides a unique spectrum of neuropathic symptoms, comprising acute motor and sensory symptoms which occur immediately following infusion, and chronic neuropathy which develops with increasing cumulative dose (Park et al., 2011). The clinical treatment of chemotherapy-induced neuropathy is still unsatisfactory. Only symptomatic drugs can be used and, in addition to the onset of side effects, their effectiveness in the management of painful neuropathy is not yet definitively proven (Hershmann et al., 2014). In this context, information regarding the pathophysiology of oxaliplatin-induced neurotoxicity is still lacking. To note, evidences collected up to now relate to several molecular and morphological changes occurring in the CNS (Di Cesare Mannelli et al., 2013; Di Cesare Mannelli et al., 2015a), suggesting a direct impact of the chemotherapy agent with central nervous compartment.

In the *in vivo* model of oxaliplatin-induced neuropathy (Di Cesare Mannelli et al., 2015b), our preliminary data showed the extravasation of ImmunoglobulinG (IgG) from the blood circulation to the lumbar spinal cord parenchyma, indicating the failure of the BSCB integrity. The immunofluorescent analysis also revealed the astrocytic activation all around the blood vessels of lumbar spinal cord region after chronic treatment with the anticancer agent. Glial cells of the CNS are mainly involved in the development and maintenance of neuropathic pain states (Marchand et al., 2005; Wieseler-Frank et al., 2004). In particular astrogliosis, occurring at both spinal and supra-spinal levels, is mainly involved in a complex response that strongly relate with the chronicity of oxaliplatin-induced painful state (Di Cesare Mannelli et al., 2013; Pacini et al., 2016). On the other hand, astrocytes are essential for the neurovascular coupling and the maintenance of the BBB homeostasis (Cabezas et al., 2014). By means of astrocytic endfeet, alterations in the endothelial compartment make astrocytes ready for compensatory responses. To note, astroglia negatively reacts to the toxic induction, harmfully altering neuronal activity. Otherwise, reactive astrogliosis induces disruption of the NVU homeostasis and drives the loss of integrity of the BBB (Argaw et al., 2009). Interestingly, the barrier integrity is compromised at both brain and

spinal cord levels during neuropathic pain conditions and this background is often accompanied by astrocytic activation (Gordh and Sharma, 2006; Echeverry et al., 2011).

In order to better understand possible changes in the permeability of both BBB and BSCB, different groups of mice, daily treated with oxaliplatin (2.4 mg kg^{-1}, *i.p.* (Di Cesare Mannelli et al., 2013)), were injected with fluorescent dye which was allowed to circulate for 15 min. The fluorescent analysis of specific brain and spinal cord regions mainly involved in the pain sensitization during oxaliplatin-induced neuropathy (Di Cesare Mannelli et al., 2013) revealed an increased permeability in the prefrontal cortex and lumbar spinal cord sites after 7 days of treatment with the anticancer agent. Otherwise, the permeability in those areas was not further increased after longer treatment (14 days) with oxaliplatin, indicating transient and reversible permeability alterations induced by the antineoplastic compound to the BBB/BSCB.

Recently, the use of coupled plasma–mass spectrometry revealed the presence of small amount of oxaliplatin (6.6 nM) in the CSF of rats once injected with the anticancer agent (Huang et al., 2016), in accordance with previous findings obtained in non-human primates (Jacobs et al., 2005). To note, Huang and colleagues highlighted that the injection of the same amount of oxaliplatin, directly in the CSF, was able to decrease the pain threshold (Huang et al., 2016). On the other hand, the plasma concentration in the rat, after repeated administration, is 18.3 μM in line to human plasma concentration (Zanardelli et al., 2014), indicating that cumulative oxaliplatin could continuously affect the BBB layer. However, to date, the molecular bases that can lead to BBB damage are unknown as well as it is not known if oxaliplatin, in addition to a modest crossing of BBB, may alter signalling in the NVU.

To investigate in detail the altered machinery of the endothelial compartment of the NVU, we set up an *in vitro* model by the using a rat brain endothelial cell line (RBE4). Oxaliplatin impaired the cell viability in dose (1-100 μM) - and time (8-24 h)-dependent manner. Thus we choose doses that could reflect the plasmatic concentrations of the anticancer agent after repeated treatment. To note, these concentrations slightly or do not impact the RBE4 vitality allowing to mimic a damage that does not permanently affect the endothelial compartment of the BBB.

One of distinguished features of oxaliplatin-induced neurotoxicity is represented by the oxidative stress, which occurs both in the PNS and the CNS tissues (Di Cesare Mannelli et al., 2012). To note, proteins particularly suffer the alteration of the oxidative cellular state. As a consequence of the modification, carbonyl groups are introduced into protein side chains by a site-specific mechanism, inducing decreased functionality (Disatnik et al., 2000). Interestingly, because oxidative protein folding occurs in the ER and perturbations in protein folding can cause deleterious consequences, alterations in redox status or generation of ROS could directly affect ER homeostasis and protein folding (Malhotra and Kaufman, 2007). GRP78/BiP (Glucose Regulated Protein 78) is a major chaperone protein critical for protein quality control of the ER, as well as controlling the activation of the ER-transmembrane signaling molecules. GRP78 levels are up-regulated under stressed conditions which leads to the accumulation of unfolded proteins (Wang et al., 2009). In RBE4, oxaliplatin strongly enhanced the expression of GRP78 after 8 h treatment suggesting the impairment of ER machinery as one of the first maladaptive response to the anticancer agent. To note, GRP78 levels, after a first restoration, are partially altered again by the higher concentration of oxaliplatin indicating the beginning of a new response of the organelle.

The ER is considered the predominant Ca^{2+} store as it contains approximately 70% of the cell's total Ca^{2+} reserve. Usually, Ca^{2+} is released following the activation Gq-protein coupled receptor (GqPCR) in the plasma membrane with subsequent activation of PLC and production of diacylglycerol and inositol 1,4,5-trisphosphate (InsP3). InsP3, in turn, binds the InsP3 receptor on the ER membrane, allowing the release of Ca^{2+} up to the cytoplasmic concentration of 1 μM (De bock et al., 2013). Notably, continuous release of Ca^{2+} from ER stores leads metabolic cellular changes and, in particular, to endothelial permeability increase (De Bock et al., 2011). To analyse possible changes in the Ca^{2+} stores content, ATP was applied, as trigger of calcium oscillations (De Bock et al., 2013) to RBE4 cells, untreated or previously treated with oxaliplatin. As result, oscillations provided by the nucleotide were significantly lower in the cells that were pre-treated with the antineoplastic compound (10 and 30 μM) for 16 h but not after 8 h. To this regard, compensatory

mechanisms, such as membrane channel opening, could allow the entry of extracellular Ca^{2+} after 8 but not after 16 h. These data were further confirmed by a second experiment where the application of thapsigargin, a non-competitive inhibitor of the sarco/endoplasmic reticulum Ca^{2+} ATPase (SERCA) once applied raises cytosolic (intracellular) calcium concentration by blocking the ability of the cell to pump calcium into the sarcoplasmic and endoplasmic reticula. However, RBE4 pretreated with oxaliplatin for 16 h showed lower $[Ca^{2+}]_i$ increase, confirming the lost of intracellular calcium stores.

Under pathological conditions, changes in ER and cytosolic Ca^{2+} homeostasis are precursor of apoptotic pathways in endothelial cells (Fonseca et al., 2013). To note, the amplification of chaperones folding capacity such as GRP78 enhances the transcription of genes for protein disulfide isomerases, CAAT/enhancer binding protein homologous protein (CHOP) and genes involved in angiogenesis and autophagy (Ameri and Harris, 2008). Furthermore, CHOP alters the levels of the pro-apoptotic factor Bax enhancing its translocation in the mitochondrion compartment with subsequent cytochrome C release and activation of the apoptosis-effector caspase-3 (Marciniak et al., 2004; Kim et al., 2006). Otherwise caspase-3 can be activated directly by GRP78 via both mitochondrion- and apoptotic-independent pathways. It is well known that the accumulation of unfolded proteins in the ER triggers the activation of the ER-resident caspase-12, which leads to the increase of caspase-9 levels, thus promoting the activation of caspase-3 (Lin et al., 2008). Oxaliplatin enhanced the activation of caspase-3 after 8 h, 16 h as well as 24 h. However BAX expression was increased only after 24 h, leading to speculate that the antineoplastic agent did not trigger apoptotic pathways unless the higher concentration used (30 μM) and longest time treatment. Intriguingly, oxaliplatin did not provoke the release of cytochrome C neither after 8 h nor 16 h, suggesting the possibility of mitochondrion-independent activation of caspase-3 at this time treatments.

In the meanwhile, oxaliplatin, dose-dependently, augmented the release of ATP in the extracellular space after 8 and 16 h. In the vascular system several pathways for ATP liberation have been proposed, including vesicular release and channel-dependent mechanisms, among which connexin hemichannels and

pannexin channels are the most studied (Lohman et al., 2012b). To note, different mechanisms have been proposed as trigger for connexin and pannexin opening under pathological conditions such as intracellular and extracellular Ca^{2+} changes, depolarization and caspase-mediated cleavage of the carboxy-terminal sequence (Lohman and Isakson, 2014; Dahl, 2015). Recently, the role of hemichannels at the BBB level, under pathological conditions, has been deeply analysed. Their opening has been relied to vascular inflammation as well as both connexins and pannexins of ECs contribute to ischemia-induced alteration at the BBB level (Kaneko et al., 2015; Wei et al., 2015). However, different release pathways of the nucleotide after oxaliplatin treatment are still under investigation.

On the other hand, the ATP plays a fundamental role in intercellular communication, in particular in the NVU (Bynoe et al., 2015). In this context, the nucleotide is a key molecule and its extracellular accumulation triggers purinergic signalling cascades in a diversity of cell types. ATP, acting on purinergic receptors of the vascular wall, the metabotropic P2Y receptors and their ionotropic P2X counterparts in the endothelial membrane cause TJs remodelling, via both Ca^{2+}-dependent and Ca^{2+}-independent pathways (Yang et al., 2016). However, other findings suggested that ATP does not alter the TJ apparatus (De Bock et al., 2011). On the other hand, the continuous release of ATP from ECs after oxaliplatin treatment could act on purinergic receptors on astrocytes and neurons affecting their homeostasis. Perpetuated activation of their purine receptors, in particular the $P2X_7$ subtype ($P2X_7R$) of the ATP-gated ionotropic P2X receptors, alters the normal crosstalk between glial and neurons leading to abnormal calcium currents which propagate along synapses (Bennett et al., 2009; Sperlagh et al., 2006). To note, evidences indicate that ATP and its purine receptors are involved in the regulation of neuropathic pain (Burnstock, 2015; Tsuda et al., 2010).

TJ transmembrane proteins are linked to the cytoskeletal platform thanks to cytoplasmic proteins, which contribute to TJ integrity. Among them, ZO proteins allow the anchorage of transmembrane TJ proteins to the cytoskeleton and drive the correct spatial distribution of claudins via the PDZ domains (Fanning et al., 2002). RBE4 treated with oxaliplatin showed altered organization of the ZO-1, at increasing both concentration and time treatment

with the antineoplastic compound. Furthermore, the distribution of cytoskeleton protein F-actin, which normally allows the correct localization of TJs, was affected by the treatment with the anticancer agent. F-actin re-localization leads to changes in centripetal cell tension, which may directly affect the adhesive property of TJs (Stamatovic et al., 2016).

This data ultimately confirm the loss of barrier integrity following treatment with oxaliplatin. As a toxic agent, oxaliplatin may trigger in the endothelial cell, metabolic and structural changes that lead to barrier function alteration. In this context, organic cationic transporters (OCT1 and OCT2) and the copper uptake transporter 1 (CTR1) could allow the entrance of the antineoplastic compound in the ECs (Wu et al., 2015; Cui et al., 2017).

Several evidence highlight that both tight junction and adherens junction remodelling is accompanied by a reorganization of perijunctional F-actin filaments resulting in the disappearance of the junctional proteins from areas of cell–cell contact (Ivanov et al., 2005). The actin cytoskeleton interacts with the motor protein myosin II right nearby the plasma membrane. Interactions between actin and myosin lead to cytoskeleton contractility and the formation of stress fibers. This is allowed by the phosphorylation of the regulatory myosin light chain (MLC) associated with myosin II. MLC phosphorylation is regulated by the non-muscle MLC kinase (MLCK), which phosphorylates MLC in a Ca^{2+}-dependent manner (De Bock et al., 2013). Notably, actin fiber stress has been shown in many types of insults such as stroke/ipoxia, alcohol exposure and E. coli infection (Haorah et al., 2008; Kim et al., 2008; Hicks et al., 2010). In this context, Ca^{2+} is a second messenger with a major role in the regulation of BBB functions (Olesen 1989). To note, $[Ca^{2+}]_i$ raise is associated with elevated permeability and decreased trans-endothelial resistance of brain endothelial cells (De Bock et al., 2013). Furthermore, experimental data suggest that oxaliplatin affects cell metabolism in complex pathways involving cytoplasmic Ca^{2+} changes (Nassini et al., 2011; Di Cesare Mannelli et al., 2016). Thus, we focused on the possibility of fast changes in $[Ca^{2+}]_i$ caused by oxaliplatin. Intriguingly, the anticancer agent was able to enhance Ca^{2+} oscillations in the ECs just after less than 10 min. Those oscillations required extracellular Ca^{2+}, leading to hypothesize the implication of membrane channels opening. To note, Panx1 channel, expressed in ECs of the brain

microvasculature, closed at resting membrane potentials could be opened by several stimuli, allowing Ca^{2+} entry (Dahl, 2015). Our data showed that oscillations triggered by oxaliplatin were decreased by the specific Panx1 blocker, ^{10}Panx, suggesting a role for the hemichannel in the raising of $[Ca^{2+}]_i$. Notably, previous data revealed that Panx1 can be functionally recruited by $P2X_7R$ during oxaliplatin-induced neuropathy. The use of Panx1 blockers permitted to prevent the glutamate release from cerebro-cortical nerve terminals as well as reduced the chemotherapy-induced neuropathic pain (Di Cesare Mannelli et al., 2015b). However, the opening of other plasma membrane channels, such as connexin hemichannels or voltage-gated calcium channels, cannot be excluded. Furthermore, oxaliplatin-triggered $[Ca^{2+}]_i$ increase is partially reduced both by the selective PLC blocker and the inhibitor of InsP3R. The InsP3 can be augmented by the increased activity of PLCβ, once triggered by the activation of GqPCRs, as above-mentioned. Otherwise, Ca^{2+} entering the cell through gap junction channels can also activate ryanodine receptors (RyRs), via a Ca^{2+}-induced Ca^{2+} release mechanism, and, in turn, facilitate the activation of PLCβ, thus increasing InsP3 levels (Thore et al., 2005). This result highlights the involvement of ER in the oxaliplatin-induced $[Ca^{2+}]_i$ alteration: continuos release of Ca^{2+} from stores induce long-term depletion of ER.

Moreover, our results showed the increased release of ATP after the brief application of oxaliplatin. Released ATP could enhance Ca^{2+} oscillations in a self-sustained GqPCRs-triggered mechanism. At the same time, perpetuated release of the nucleotide could qickly alter the BBB homeostasis and trigger altered signalling in the NVU.

Finally, both ZO-1 relocation and F-actin cytoskeleton remodelling was seen after 10 min treatment with the antineoplastic compound indicating that TJs alteration occurs very quickly and allowing to speculate fast changes in the permeability of BBB endothelial compartment. This event may require coordinated response between neighbouring ECs. In this context, the propagation of Ca^{2+} signalling along the endothelial layer could explain, at least in part, quick and transient changes in permeability. Particularly, two mechanisms have been highlighted to explain intercellular Ca^{2+} dynamics: one is based on the direct passage of Ca^{2+} and InsP3 throughout gap junctions

channels of two adjacent cells. The second pathway involves the release of paracrine components (generally ATP), which, once diffused in the extracellular space, binds the corresponding GqPCRs on neighbouring cells, triggering cascades that evoke $[Ca^{2+}]_i$ increase (Leybaert and Sanderson, 2012; Wang et al., 2013).

In conclusion, our data reveal the pathophysiological involvement of BBB's endothelial compartment in oxaliplatin-induced neurotoxicity. These results are part of the complicated picture of alterations that occur during and after chemotherapy treatment. In this context, changes in ECs following exposure to the platinum derivative, both in the acute and in the chronic phase, would not only explain the passage of small amounts of oxaliplatin, but would lead to the activation of the entire NVU, thus causing the profound alterations, which occur at spinal and supra-spinal levels of the CNS. With this regards, rapid modification of $[Ca^{2+}]_i$ and ATP release are the basis of modification both in the fast and long-term response to the anticancer agent. Even though, mechanisms underlying the modification in the ECs and the signalling cascades triggered in the surrounding environments need deeper examinations, the endothelial compartment of BBB plays a relevant role in the pathophysiology of oxaliplatin-induced neuropathy.

6. Bibliography

- Abbott, NJ, Patabendige, AA, Dolman, DE, Yusof, SR, Begley, DJ. Structure and function of the blood-brain barrier. Neurobiol Dis. 2010; 37(1):13-25.
- Abbott, NJ and Friedman, A. Overview and introduction: the blood-brain barrier in health and disease. Epilepsia; 2012; 53: 1-6.
- Abbott, NJ, Ronnback, L, and Hansson, E. Astrocyte endothelial interactions at the blood-brain barrier. Nature Reviews Neuroscience. 2006; 7(1): 41-53.
- Abbott, NJ. Dynamics of CNS barriers: evolution, differentiation, and modulation. Cell. Mol. Neurobiol. 2005; 25: 5-23.
- Abbott, NJ. Blood-brain barrier structure and function and the challenges for CNS drug delivery. J Inherit Metab Dis. 2013; 36(3): 437-49.
- Allegra, CJ, Yothers, G, O'Connell, MJ, et al. Initial safety report of NSABP C-08: a randomized phase III study of modified FOLFOX6 with or without bevacizumab for the adjuvant treatment of patients with stage II or III colon cancer. J Clin Oncol. 2009; 27: 3385-90.
- Alvarez, J, et al. Glial influence on the blood brain barrier. Glia. 2013; 61, 1939-1958.
- Ameri, K, Harris, AL. Activating transcription factor 4, Int J Biochem Cell Biol. 2008; 40: 14-21.
- American Cancer Society. Cancer Facts & Figures. Atlanta: *American Cancer Society;* 2009.
- Anderson, CM, Nedergaard, M. Astrocyte-mediated control of cerebral microcirculation. Trends Neurosci. 2003; 26(7): 340-344.
- Andrè, T, Boni, C, Mounedji-Boudiaf, L, Mounedji-Boudiaf, L, Navarro, M, Tabernero, J, Hickish, T, Topham, C, Zaninelli, M, Clingan, P, Bridgewater, J, Tabah-Fisch, I, de Gramont, A. Oxaliplatin, fluorouracil, and leucovorin as adjuvant treatment for colon cancer. N Engl J Med. 2004; 350: 2343-51.
- Andrè, T, Boni, C, Navarro, M, Tabernero, J, Hickish, T, Topham, C, Bonetti, A, Clingan, P, Bridgewater, J, Rivera, F, de Gramont, A. Improved overall survival with oxaliplatin, fluorouracil, and leucovorin

as adjuvant treatment in stage II or III colon cancer in the MOSAIC trial. J Clin Oncol. 2009; 27: 3109-16.

- Argaw, AT, Gurfein, BT, Zhang, Y, Zameer, A, John, GR. VEGF-mediated disruption of endothelial CLN-5 promotes blood-brain barrier breakdown. Proc Natl Acad Sci U S A. 2009; 106(6): 1977–1982.
- Argyriou, AA, Polychronopoulos, P, Iconomou, G, Koutras, A, Makatsoris, T, Gerolymos, MK, Gourzis, P, Assimakopoulos, K, Kalofonos, HP, Chroni, E. Incidence and characteristics of peripheral neuropathy during oxaliplatin-based chemotherapy for metastatic colon cancer. Acta Oncol. 2007; 46(8): 1131-7.
- Armstead, WM and Raghupathi, R. Endothelin and the neurovascular unit in pediatric traumatic brain injury. Neurol Res. 2011; 33: 127–132.
- Armulik A et al. Pericytes regulate the blood–brain barrier. Nature 2010; 468: 557–561.
- Armulik, A, Abramsson, A, and Betsholtz, C. Endothelial/pericyte interactions. Circ. Res. 2005; 97: 512–523.
- Avan, A, Postma, TJ, Ceresa, C, Avan, A, Cavaletti, G, Giovannetti, E, Peters, GJ. Platinum-induced neurotoxicity and preventive strategies: Past, present, and future. Oncologist. 2015; 20(4): 411-32.
- Baranova, A, Ivanov, D, Petrash, N, Pestova, A, Skoblov, M, Kelmanson, I, Shagin, D, Nazarenko, S, Geraymovych, E, Litvin, O, Tiunova, A, Born, TL, Usman, N, Staroverov, D, Lukyanov, S, Panchin, Y. The mammalian pannexin family is homologous to the invertebrate innexin gap junction proteins. Genomics. 2004; 83: 706-16.
- Bazzoni, G and Dejana, E. Endothelial cell-to-cell junctions: molecular organization and role in vascular homeostasis. Physiol Rev. 2004; 84(3): 869-901.
- Bazzoni, G. Pathobiology of junctional adhesion molecules. Antioxid Redox Signal. 2011; 15: 1221-1234.
- Bell, RD, Winkler, EA, Sagare, AP, Singh, I, Larue, B, Deane, R et al. Pericytes control key neurovascular functions and neuronal phenotype in the adult brain and during brain aging. Neuron 68, 2010: 409–427.

- Bennett, MR, Farnell, L, Gibson, WG. P2X7 regenerative-loop potentiation of glutamate synaptic transmission by microglia and astrocytes. J Theor Biol. 2009; 261: 1-16.
- Bhalla-Gehi, R, Penuela, S, Churko, JM, Shao, Q, Laird, DW. Pannexin1 and pannexin3 delivery, cell surface dynamics, and cytoskeletal interactions. J Biol Chem. 2010; 285: 9147-60.
- Boassa, D, Ambrosi, C, Qiu, F, Dahl, G, Gaietta, G, Sosinsky, G. Pannexin1 channels contain a glycosylation site that targets the hexamer to the plasma membrane. J Biol Chem. 2007; 282: 31733-43.
- Bonkowski, D et al. The CNS microvascular pericyte: pericyte-astrocyte crosstalk in the regulation of tissue survival. Fluids BarriersCNS. 2011; 8: 8.
- Bradford, MM. A rapid and sensitive method for the quantitation of microgram quantities of protein utilizing the principle of protein-dye binding. Anal Biochem. 1976; 72: 248-54.
- Brisset, AC, Isakson, BE, Kwak, BR. Connexins in vascular physiology and pathology. Antioxid Redox Signal. 2009; 11(2): 267-82.
- Bruzzone, R, Hormuzdi, SG, Barbe, MT, Herb, A, Monyer, H. Pannexins, a family of gap junction proteins expressed in brain. Proc Natl Acad Sci. 2003; 100: 13644-9.
- Bynoe, MS, Viret, C, Yan, A, Kim, DG. Adenosine receptor signaling: a key to opening the blood–brain door. Fluids Barriers CNS. 2015; 12:20.
- Cabezas, R, Ávila, M Gonzalez, J, El-Bachá,, RS, Báez, E et al. Astrocytic modulation of blood brain barrier: perspectives on Parkinson's disease. Front Cell Neurosci. 2014; 8: 211.
- Carlton, SM, Du, J, Tan, HY, Nesic, O, Hargett, GL, Bopp, AC, Yamani, A, Lin, Q, Willis, WD, Hulsebosch, CE. Peripheral and central sensitization in remote spinal cord regions contribute to central neuropathic pain after spinal cord injury. Pain. 2009; 147: 265-76.
- Castejón, OJ. Ultrastructural pathology of cortical capillary pericytes in human traumatic brain oedema. FoliaNeuropathol. 2011; 49: 162-173.

- Cavaletti, G, Tredic, G, Petruccioli, MG, Dondè, E, Tredici, P, Marmiroli, P, Minoia, C, Ronchi, A, Bayssas, M, Etienne, GG. Effects of different schedules of oxaliplatin treatment on the peripheral nervous system of the rat. Eur J Cancer. 2001; 37(18): 2457-63.
- Choi, BS, Zheng, W. Copper transport to the brain by the blood-brain barrier and blood-CSF barrier. Brain Res. 2009; 1248: 14-21.
- Conroy, T, Desseigne, F, Ychou, M, et al. Randomized phase III trial comparing FOLFIRINOX (F: 5FU/leucovorin [LV], irinotecan [I], and oxaliplatin [O]) versus gemcitabine (G) as first-line treatment for metastatic pancreatic adenocarcinoma (MPA): preplanned interim analysis results of the PRODIGE 4/ACCORD 11 trial. J Clin Oncol, 2010; 28(suppl): 15 (abstract 4010).
- Cruciani, V, Mikalsen, SO. The vertebrate connexin family. Cell Mol Life Sci. 2006; 63: 1125-40.
- Cui, H, Zhang, AJ, McKeage, MJ, Nott, LM, Geraghty, D, Guven, N, Liu, JJ. Copper transporter 1 in human colorectal cancer cell lines: Effects of endogenous and modified expression on oxaliplatin cytotoxicity. J Inorg Biochem. 2017; pii: S0162-0134 (17) 30158-7.
- Dahl, G. ATP release through pannexon channels. Philos Trans R Soc Lond B Biol Sci. 2015; 370 (1672).
- Dalkara, T, Gursoy-Ozdemir, Y and Yemisci, M. Brain microvascular pericytes in health and disease. Acta Neuropathol. 2011; 122: 1–9.
- Daneman, R, Agalliu, D, Zhou, L, Kuhnert, F, Kuo, CJ and Barres, BA. Wnt/beta-catenin signaling is required for CNS, but not non-CNS, angiogenesis. Proc Natl Acad Sci. U.S.A. 2009; 106: 641–646.
- Daneman, R, Zhou, L, Kebede, AA and Barres, BA. Pericytes are required for blood-brain barrier integrity during embryogenesis. Nature. 2010; 468: 562-566.
- Daneman, R. The blood-brain barrier in health and disease. Ann.Neurol. 2012; 72: 648-672.
- De Bock, M, Culot, M, Wang, N, Bol, M, Decrock, E, De Vuyst, E, da Costa, A, Dauwe, I, Vinken, M, Simon, AM, Rogiers, V, De Ley, G, Evans, WH, Bultynck, G, Dupont, G, Cecchelli, R, Leybaert L.

Connexin channels provide a target to manipulate brain endothelial calcium dynamics and blood–brain barrier permeability. J Cereb Blood Flow Metab. 2011; 31(9): 1942-1957.

- De Bock, M, Wang, N, Decrock, E, Bol, M, Gadicherla, AK, Culot, M, Cecchelli, R, Bultynck, G, Leybaert, L. Endothelial calcium dynamics, connexin channels and blood–brain barrier function. Prog Neurobiol. 2013; 108: 1-20.
- de Gramont, A, Figer, A, Seymour, M, et al. Leucovorin and fluorouracil with or without oxaliplatin as first-line treatment in advanced colorectal cancer. J Clin Oncol 2000; 18: 2938-47.
- de Gramont, A, Vignoud, J, Tournigand, C, et al. Oxaliplatin with high-dose leucovorin and 5-fluorouracil 48-hour continuous infusion in pretreated metastatic colorectal cancer. Eur J Cancer. 1997; 33: 214-9.
- de Gramont, A, Cervantes, A, Andre, T, et al. OPTIMOX study: FOLFOX7/ LV5FU2 compared to FOLFOX 4 in patients with advanced colorectal cancer. Proc Am Soc Clin Oncol 2004; 23: 251.
- De Vuyst, E, Wang, N, Decrock, E, De Bock, M, Vinken, M, Van Moorhem, M, Lai, C, Culot, M, Rogiers, V, Cecchelli, R, Naus, CC, Evans, WH, Leybaert, L. Ca^{2+} regulation of connexin43 hemichannels in C6 glioma and glial cells. Cell Calcium. 2009; 46(3): 176-187.
- Del Zoppo, GJ. The neurovascular unit in the setting of stroke. J Intern Med. 2010; 267: 156–171.
- Devaskar, S, Zahm, DS, Holtzclaw, L, Chundu, K, Wadzinski, BE. Developmental regulation of the distribution of rat brain insulin-insensitive (Glut 1) glucose transporter. Endocrinology. 1991; 129: 1530–1540.
- Di Cesare Mannelli, L, Pacini, A, Bonaccini, L, Zanardelli, M, Mello, T, Ghelardini, C. Morphologic features and glial activation in rat oxaliplatin-dependent neuropathic pain. J Pain. 2013; 14(12): 1585-600.
- Di Cesare Mannelli, L, Pacini, A, Corti, F, Boccella, S, Luongo, L, Esposito, E, Cuzzocrea, S, Maione, S, Calignano, A, Ghelardini, C.

Antineuropathic profile of N-palmitoylethanolamine in a rat model of oxaliplatin-induced neurotoxicity. PLoS One. 2015a; 10(6): e0128080.

- Di Cesare Mannelli, L, Pacini, A, Micheli, L, Tani, A, Zanardelli, M, Ghelardini C. Glial role in oxaliplatin-induced neuropathic pain. Exp Neurol. 2014; 261: 22–33.
- Di Cesare Mannelli, L, Zanardelli, M, Failli P, Ghelardini, C. Oxaliplatin-induced neuropathy: oxidative stress as pathological mechanism. Protective effect of silibinin. J Pain. 2012; 13(3): 276-84.
- Di Cesare Mannelli, L, Marcoli, M, Micheli, L, Zanardelli, M, Maura, G, Ghelardini, C, Cervetto, C. Oxaliplatin evokes P2X7-dependent glutamate release in the cerebral cortex: A pain mechanism mediated by Pannexin 1. Neuropharmacology. 2015b; 97:133-41.
- Di Cesare Mannelli, L, Zanardelli, M, Landini, I, Pacini, A, Ghelardini, C, Mini, E, Bencini, A, Valtancoli, B, Failli, P. Effect of the SOD mimetic MnL4 on in vitro and in vivo oxaliplatin toxicity: Possible aid in chemotherapy induced neuropathy. Free Radic Biol Med. 2016; 93: 67-76.
- Di Francesco, AM, Ruggiero, A, Riccardi, R. Cellular and molecular aspects of drugs of the future: oxaliplatin. Cell Mol Life Sci. 2002; 59(11): 1914-27.
- Disatnik, M, Chamberlain, JS, Rando, TA. Dystrophin mutations predict cellular susceptibility to oxidative stress. Muscle Nerve 2000; 23: 784-792.
- Echeverry, S, Shi, XQ, Rivest, S and Zhang, J. Peripheral nerve injury altersblood-spinal cordbarrier functional andmolecular integrity through a selective inflammatory pathway. Journal of Neuroscience. 2011; 31(30): 10819–10828.
- Esteban-Fernández, D, Moreno-Gordaliza, E, Cañas, B, Palacios, MA and Gomez-Gómez, MM. Analytical methodologies for metallomics studies of antitumor Pt-containing drugs. Metallomics. 2010; 2: 19-38.
- Fanning, AS, Ma, TY, Anderson, JM. Isolation and functional characterization of the actin binding region in the tight junction protein ZO-1. FASEB J. 2002; 16: 1835–1837.

- Figley, CR, Stroman, PW. The role(s) of astrocytes and astrocyte activity in neurometabolism, neurovascular coupling, and the production of functional neuroimaging signals. Eur J Neurosci. 2011; 33(4): 577-88.
- Figueroa, XF, Lillo, MA, Gaete, PS, Riquelme, MA, Saez, JC. Diffusion of nitric oxide through cell membranes of the vascular wall requires specific connexin-based channels, Neuropharmacology. 2013; 75: 471-478.
- Filosa, JA, Bonev, AD, Nelson, MT. Calcium dynamics in cortical astrocytes and arterioles during neurovascular coupling. Circ Res. 2004: 95(10), 73-81.
- Fonseca, AC, Ferreiro, E, Oliveira, CR, Cardoso, SM, Pereira, CF. Activation of the endoplasmic reticulum stress response by the amyloid-beta 1-40 peptide in brain endothelial cells. Biochim Biophys Acta. 2013; 1832(12): 2191-203.
- Gaete, PS, Lillo, MA, Figueroa, XF. Functional role of connexins and pannexins in the interaction between vascular and nervous system. J Cell Physiol. 2014; 229 (10): 1336-45.
- Gamelin, E, Gamelin, L, Bossi, L, Quasthoff, S. Clinical aspects and molecular basis of oxaliplatin neurotoxicity: Current management and development of preventive measures. Semin Oncol 2002; 29: 21-33.
- Gordh, T and Sharma, HS. Chronic spinal nerve ligation induces microvascular permeability disturbances, astrocytic reaction, and structural changes in the rat spinal cord. ActaNeurochir. 2006; Suppl. 96: 335–340.
- Gordh, T, Chu, H and Sharma, HS. Spinal nerve lesion alters blood-spinal cord barrier function and activates astrocytes in the rat. Pain, 2006; 124 (1-2): 211–221.
- Gordon, GRJ, Mulligan, SJ and Mac Vicar, BA. Astrocyte control of the cerebrovasculature. Glia 2007; 55: 1214-1221.
- Graham, MA, Lockwood, GF, Greenslade, D, Brienza, S, Bayssas, M, et al. Clinical pharmacokinetics of oxaliplatin: a critical review. Clin Cancer Res. 2002; 6: 1205–1218.

- Grammas, P, Martinez, J and Miller, B.Cerebral microvascular endothelium and the pathogenesis of neurodegenerative diseases. Expert Rev Mol Med. 2011;13: e19.
- Greenwood, J, Amos, CL, Walters, CE, Couraud, P-O, Lyck, R, Engelhardt, B. Intracellular domain of brain endothelial intercellular adhesion molecule-1 is essential for T lymphocyte-mediated signaling and migration. J Immunol. 2003; 171: 2099 2108.
- Grolleau, F, Gamelin, L, Boisdron-Celle M, et al. A possible explanation for a neurotoxic effect of the anticancer agent oxaliplatin on neuronal voltage-gated sodiumchannels. J Neurophysiol. 2001; 85: 2293-7.
- Grothey, A, and Goldberg, RM. A review of oxaliplatin and its clinical use in colorectal cancer. Expert Opin Pharmacother. 2004; 5: 2159-70.
- Hamilton, NB, Attwell, D and Hall, CN. Pericyte-mediated regulation of capillary diameter: a component of neurovascular coupling in health and disease. Front. Neuroenergetics. 2010; 2: 5.
- Han, CH, Khwaounjoo, P, Kilfoyle, DH, Hill, A, McKeage, MJ. Phase I drug-interaction study of effects of calcium and magnesium infusions on oxaliplatin pharmacokinetics and acute neurotoxicity in colorectal cancer patients. BMC Cancer. 2013; 13: 495.
- Hanstein, R, Hanani, M, Scemes, E, Spray, DC. Glial pannexin1 contributes to tactile hypersensitivity in a mouse model of orofacial pain. Sci Rep. 2016; 6: 38266.
- Haorah, J, Schall, K, Ramirez, SH, Persidsky, Y. Activation of protein tyrosine kinases and matrix metalloproteinases causes blood-brain barrier injury: novel mechanism for neurodegeneration associated with alcohol abuse. Glia. 2008; 56, 78-88.
- Harder, DR, Zhang, C and Gebremedhin, D. Astrocytes function in matching blood flow to metabolic activity. News Physiol Sci. 2002; 17: 27–31.
- Haseloff, RF et al. In search of the astrocytic factor(s) modulating blood-brain barrier functions in brain capillary endothelial cells in vitro. Cell.Mol.Neurobiol. 2005; 25, 25–39.

- Hawkins, BT and Davis TP. The blood-brain barrier/neurovascular unit in health and disease. Pharmacol.Rev. 2005; 57: 173–185.
- Hayat, MJ, Howlader, N, Reichman, ME, Edwads, BK. Cancer statistics, trends, and multiple cancer analyses from the surveillance, epidemiology, and end results (Seer) program. Oncologist. 2007; 12: 20-37.
- Hershmann, DL, Lacchetti, C, Dworkin, RH, Lavoie Smith, EM, Bleeker, J, Cavaletti, G, Chauhan, C, Gavin, P, Lavino, A, Lustberg, MB, Paice J, Schneider, B, Smith ML, Smith, T, Terstriep S, Wagner-Johnston, N, Bak, K, Loprinzi, CL. American Society of Clinical Oncology. Prevention and management of chemotherapy-induced peripheral neuropathy in survivors of adult cancers: American Society of Clinical Oncology clinical practice guideline. J Clin Oncol. 2014; 32: 1941-1967.
- Hicks, K, O'Neil, RG, Dubinsky, WS, Brown, RC. Trpc-mediated actin- Q myosin contraction is critical for Bbb disruption following hypoxic stress. American Journal of Physiology. Cell Physiology. 2010. 298(6): C1583-C1593.
- Hol, EM, and Pekny, M. Glial fibrillary acidic protein (GFAP) and the astrocyte intermediate filament system in diseases of the central nervous system. Curr Opin Cell Biol. 2015; 32: 121-30.
- Huang, ZZ, Li ,D, Ou-Yang, HD, Liu, CC, Liu, XG, Ma, C, Wei, JY, Liu, Y, Xin, WJ. Cerebrospinal fluid oxaliplatin contributes to the acute pain induced by systemic administration of oxaliplatin. Anesthesiology. 2016; 124(5): 1109-21.
- Huber, JD, Hau, VS, Borg, L, Campos, CR, Egleton, RD and Davis, TP. Blood-brain barrier tight junctions are altered during a 72-h exposure to λ carrageenan-induced inflammatory pain. American Journal of Physiology - Heart and Circulatory Physiology. 2002; 283 (4): H1531–H1537.
- Ikenouchi, J, Furuse, M, Furuse, K, Sasaki, H, Tsukita, S. Tricellulin constitutes a novel barrier at tricellular contacts of epithelial cells. J Cell Biol 2005; 171: 939–945.

- Ivanov, AI, Hunt, D, Utech, M, Nusrat, A, Parkos, CA. Differential roles for actin polymerization and a myosin II motor in assembly of the epithelial apical junctional complex. Molecular Biology of the Cell. 2005; 16: 2636-2650.
- Jacobs, S, McCully, CL, Murphy, RF, Bacher, J, Balis, FM, Fox, E. Extracellular fluid concentrations of cisplatin, carboplatin, and oxaliplatin in brain, muscle, and blood measured using microdialysis in nonhuman primates. Cancer Chemother Pharmacol. 2010; 65(5): 817-24.
- Jacobs, SS, Fox E, Dennie C, Morgan LB, McCully CL, Balis FM. Plasma and cerebrospinal fluid pharmacokinetics of intravenous oxaliplatin, cisplatin, and carboplatin in nonhu an primates. Clin Cancer Res. 2005; 11: 1669-1674.
- Jing, Y, Jing, X, Yifan, Y and Bangwei, C. Oxaliplatin-Based Doublets Versus Cisplatin or Carboplatin-Based Doublets in the First-Line Treatment of Advanced Nonsmall Cell Lung Cancer. Medicine (Baltimore). 2015; 94(27): e1072
- Kalofonos, HP, et al. Irinotecan or oxaliplatin combined with leucovorin and 5-fluorouracil as first-line treatment in advanced colorectal cancer: a multicenter, randomized, phase II study. Ann Oncol 2005; 16(6): 869–877.
- Kaneko, Y, Tachikawa, M, Akaogi, R, Fujimoto, K, Ishibashi, M, Uchida, Y, Couraud, PO, Ohtsuki, S, Hosoya, K, Terasaki, T. Contribution of pannexin 1 and connexin 43 hemichannels to extracellular calcium-dependent transport dynamics in human blood-brain barrier endothelial cells. J Pharmacol Exp Ther. 2015; 353(1): 192-200.
- Kannarkat, G, Lasher, EE, Schiff, D. Neurologic complications of chemotherapy agents. Curr Op Neurol. 2007; 20: 719–725.
- Kim, JH, Kim, JH, Yu, YS, Kim, DH and Kim, KW. Recruitment of pericytes and astrocytes is closely related to the formation of tight junction in developing retinal vessels. J. Neurosci. Res. 2009; 87: 653–659.

- Kim, R, Emi, M, Tanabe, K, Murakami, S. Role of the unfolded protein response in cell death. Apoptosis. 2006; 11: 5–13.
- Kim, YV, Pearce, D, Kim, KS. Ca(2+)/calmodulin-dependent invasion of microvascular endothelial cells of human brain by Escherichia coli K1. Cell and Tissue Research. 2008; 332: 427–433.
- Koehler, RC, Roman, RJ, Harder, DR. Astrocytes and the regulation of cerebral blood flow. Trends Neurosci. 2009; 32(3): 160-169.
- Kowiański, P, Lietzau, G, Steliga, A, Waśkow, M, Moryś, J. The astrocytic contribution to neurovascular coupling--still more questions than answers? Neurosci Res. 2013; 75(3): 171-83.
- Land, SR, Kopec, JA, Cecchini, RS, Ganz, PA, Wieand, HS, Colangelo, LH, Murphy, K, Kuebler, JP, Seay, TE, Needles, BM, Bearden, JD, Colman, LK, Lanier, KS, Pajon, ER, Cella, D, Smith, RE, O'Connell, MJ, Costantino, JP, Wolmark, N. Neurotoxicity from oxaliplatin combined with weekly bolus fluorouracil and leucovorin as surgical adjuvant chemotherapy for stage II and III colon cancer: NSABP C-07. J Clin Oncol. 2007; 25(16): 2205-2211.
- Lange, S, Trost, A, Tempfer, H, Bauer, HC, Bauer, H, Rohde, E et al. Brain pericyte plasticity as a potential drug target in CNS repair. Drug Discov Today. 2013; 18: 456–463.
- Lau, LW et al. Pathophysiology of the brain extracellular matrix: a new target for remyelination. Nat.Rev.Neurosci. 2013; 14: 722–729.
- Leybaert, L, Sanderson, MJ. Intercellular Ca^{2+} waves: mechanisms and function. Physiological Reviews. 2012; 92: 1359-1392.
- Leybaert, L. Neurobarrier coupling in the brain: a partner of neurovascular and neurometabolic coupling? J. Cereb. Blood Flow Metab. 2005; 25(1): 2-16.
- Li, ZH, Zheng, R, Chen, JT, Jia, J, Qiu, M. The role of copper transporter ATP7A in platinum-resistance of esophageal squamous cell cancer (ESCC). J Cancer. 2016; 7(14): 2085-2092.
- Lin, JH, Walter, P, Yen, TS. Endoplasmic reticulum stress in disease pathogenesis. Annu Rev Pathol. 2008; 3: 399–425.
- Locovei, S, Scemes, E, Qiu, F, Spray, DC, Dahl, G. Pannexin1 is part

of the pore forming unit of the P2X7 receptor death complex. FEBS Lett. 2007; 581: 483-8.

- Locovei, S, Wang, J, Dahl, G. Activation of pannexin 1 channels by ATP through P2Y receptors and by cytoplasmic calcium. FEBS Lett. 2006; 580: 239-44.
- Lohman, AW, Billaud, M, Isakson, BE. Mechanisms of ATP release and signalling in the blood vessel wall. Cardiovasc Res. 2012a; 95(3): 269-80.
- Lohman, AW, Billaud, M, Straub, AC, Johnstone, SR, Best, AK, Lee, M, Barr, K, Penuela, S, Laird, DW, Isakson, BE. Expression of pannexin isoforms in the systemic murine arterial network. J Vasc Res. 2012b; 49(5): 405-16.
- Lohman, AW, Isakson, BE. Differentiating connexin hemichannels and pannexin channels in cellular ATP release. FEBS Lett. 2014; 588(8): 1379-88.
- Lohman, AW, Leskov, IL, Butcher, JT, Johnstone, SR, Stokes, TA, Begandt, D, De Lalio, LJ, Best, AK, Penuela, S, Leitinger, N, et al. Pannexin 1 channels regulate leukocyte emigration through the venous endothelium during acute inflammation. Nat Commun. 2015; 6: 7965.
- Lonardi, S, Sobrero, A, Rosati, G, Di Bartolomeo, M, Ronzoni, M, Aprile, G, Scartozzi, M, Banzi, M, Zampino, MG, Pasini, F, Marchetti, P, Cantore, M, Zaniboni, A, Rimassa, L, Ciuffreda, L, Ferrari, D, Barni, S., Zagonel, V, Maiello, E, Rulli, E, Labianca, R. TOSCA (Three or Six Colon Adjuvant) Investigators, 2016. Phase III trial comparing 3-6 months of adjuvant FOLFOX4/XELOX in stage II-III colon cancer: safety and compliance in the TOSCA trial, 2016. Ann Oncol. 27(11): 2074-2081.
- Luissint, AC, Artus, C, Glacial, F, Ganeshamoorthy, K and Couraud PO. Tight junctions at the blood brain barrier: physiological architecture and disease-associated dysregulation. Fluids Barriers CNS. 2012; 9: 23.
- Machover, D, Diaz-Rubio, E, de Gramont, A, et al. Two consecutive phase II studies of oxaliplatin (L-OHP) for treatment of patients with

advanced colorectal carcinoma who were resistant to previous treatment with fluoropyrimidines. Ann Oncol. 1997; 7: 95-8.

- Maindrault-Goebel, F, de Gramont, A, Louvet, C, et al. High-dose intensity oxaliplatin added to the simplified bimonthly leucovorin and 5-fluorouracil regimen as second-line therapy for metastatic colorectal cancer (FOLFOX 7). Eur J Cancer 2001; 37: 1000-1005.
- Malhotra JD, Kaufman RJ. Endoplasmic reticulum stress and oxidative stress: a vicious cycle or a double-edged sword? Antioxid Redox Signal. 2007; 9(12): 2277-93.
- Maragakis, NJ, Rothstein, JD. Mechanisms of disease: astrocytes in neurode generative disease. Nat. Clin. Pract. Neurol. 2006; 2: 679–689.
- Marchand, F, Perretti, M, McMahon, SB. Role of the immune system in chronic pain. Nat Rev Neurosci. 2005; 6: 521-532.
- Marciniak, SJ, Yun, CY, Oyadomari, S, Novoa, I, Zhang, Y, Jungreis, R, Nagata, K, Harding, HP, Ron, D. CHOP induces death by promoting protein synthesis and oxidation in the stressed endoplasmic reticulum, Genes Dev. 2004; 18: 3066–3077.
- McCaffrey, G, Seelbach, MJ, Staatz, WD, Nametz, N, Quigley, C, Campos CR, Brooks, TA, Davis, TP. Occludin oligomeric assembly at tight junctions of the blood–brain barrier is disrupted by peripheral inflammatory hyperalgesia. J Neurochem 2008; 106: 2395–2409.
- McGrath, JC and Lilley, E. Implementing guidelines on reporting research using animals (ARRIVE etc.): new requirements for publication in BJP. Br J Pharmacol. 2015; 172 (13): 3189-93.
- Miquerol, L, Thireau, J, Bideaux, P, Sturny, R, Richard, S, Kelly, RG. Endothelial plasticity drives arterial remodeling within the endocardium after myocardial infarction. Circ Res. 2015; 116(11): 1765–71.
- Mokgokong, R, Wang, S,Taylor, CJ, Barrand, MA and Hladky, SB. Ion transporters in brain endothelial cells that contribute to formation of brain Interstitial fluid. PflugersArch. 2014; 466: 887–901.
- Morgan, L, Shah, B, Rivers, LE, Barden, L, Groom, AJ, Chung, R, Higazi, D, Desmond, H, Smith, T, and Staddon, JM. Inflammation and dephosphorylation of the tight junction protein occludin in an

experimental model of multiple sclerosis. Neuroscience. 2007; 147: 664–673.

- Muoio, V, Persson, PB, Sendeski, MM. The neurovascular unit - concept review. Acta Physiol (Oxf). 2014; 210(4):790-8.
- Nag, S, Begley, DJ. Blood–brain barrier, exchange of metabolites and gases. In: Kalimo, H. (Ed.), Pathology and Genetics. Cerebrovascular Diseases. ISN Neuropath. Press. Basel. 2005; pp. 22–29.
- Nag, S. Morphology and properties of brain endothelial cells. Methods Mol. Biol. 2011; 686: 3–47.
- Nassini, R, Gees, M, Harrison, S, De Siena, G, Materazzi, S, Moretto, N, Failli, P, Preti, D, Marchetti, N, Cavazzini, A, Mancini, F, Pedretti, P, Nilius, B, Patacchini, R, Geppetti, P. Oxaliplatin elicits mechanical and cold allodynia in rodents via TRPA1 receptor stimulation. Pain. 2011; 152(7): 1621-31.
- NCCN Oncology Practice Guidelines in Oncology. Oesophageal Cancer version 2-2009.
- Nixon, RA, Lewis, SE, Marotta CA. Posttranslational modification of neurofilament proteins by phosphate during axoplasmic transport in retinal ganglion cell neurons. J Neurosci. 1987; 7: 1145-1158.
- Nordlinger, B, Sorbye, H, Glimelius, B. Poston, GJ, Schlag, PM, Rougier, P, Bechstein et al.; EORTC Gastro-Intestinal Tract Cancer Group; Cancer Research UK; Arbeitsgruppe Lebermetastasen und–tumoren in der Chirurgischen Arbeitsgemeinschaft Onkologie (ALM-CAO); Australasian Gastro-Intestinal Trials Group (AGITG); Fédération Francophone de Cancérologie Digestive (FFCD). Perioperative chemotherapy with FOLFOX4 and surgery versus surgery alone for resectable liver metastases from colorectal cancer (EORTC Intergroup trial 40983): a randomised controlled trial. Lancet. 2008; 371: 1007-16.
- Olesen, SP. An electrophysiological study of microvascular permeability and its modulation by chemical mediators. ACTA Physiologica Scandinavica. 1989; Supplement 579: 1-28.

- Pacini, A, Micheli, L, Maresca, M, Branca, JJ, McIntosh, JM, Ghelardini, C, Di Cesare Mannelli, L. The α9α10 nicotinic receptor antagonist α-conotoxin RgIA prevents neuropathic pain induced by oxaliplatin treatment. Exp. Neurol. 2016; 282: 37-48.
- Panchin, Y, Kelmanson, I, Matz, M, Lukyanov, K, Usman, N, Lukyanov, S. A ubiquitous family of putative gap junction molecules. Curr Biol. 2000; 10: 473-4.
- Park, SA, Choi, KS, Bang, JH, Huh, K, Kim, SU: Cisplatin-induced apoptotic cell death in mouse hybrid neurons is blocked by antioxidants through suppression of cisplatinmediated accumulation of p53 but not of Fas/Fas ligand. J Neurochem. 2000; 75: 946-953.
- Park, SB, Lin, CS, Krishnan, AV, Goldstein, D, Friedlander, ML, Kiernan, MC. Long-term neuropathy after oxaliplatin treatment: challenging the dictum of reversibility. Oncologist. 2011; 16(5): 708-16.
- Pelegrin, P, Surprenant, A. Pannexin-1 mediates large pore formation and interleukin-1beta release by the ATP-gated P2X7 receptor. Embo J. 2006; 25: 5071-82.
- Penuela, S, Bhalla, R, Nag, K, Laird, DW. Glycosylation regulates pannexin intermixing and cellular localization. Mol Biol Cell. 2009; 20: 4313-23.
- Peppiatt, CM, Howarth, C, Mobbs, P and Attwell, D. Bidirectional control of CNS capillary diameter by pericytes. Nature. 2006; 443: 700–704.
- Phelan, P, Bacon, JP, Davies, JA, Stebbings, LA, Todman, MG, Avery, L, Baines, RA, Barnes, TM, Ford, C, Hekimi, S, Lee, R, Shaw, JE, Starich, TA, Curtin, KD, Sun, YA, Wyman, RJ. Innexins: a family of invertebrate gap-junction proteins. Trends Genet. 1998; 14: 348-9.
- Pogoda, K, Fuller, M, Pohl, U, Kameritsch, P. NO, via its target Cx37, modulates calcium signal propagation selectively at myoendothelial gap junctions. Cell Commun Signal. 2014; 12: 33.

- Radu, BM, Bramanti, P, Osculati, F, Flonta, ML, Radu, M, Bertini, G, Fabene, PF. Neurovascular unit in chronic pain. Mediators Inflamm. 2013; 2013: 648268.
- Renn, CL, Carozzi, VA, Rhee, P, Gallop, D, Dorsey, SG, Cavaletti, G. Multimodal assessment of painful peripheral neuropathy induced by chronic oxaliplatin-based chemotherapy in mice. Mol. Pain. 2011; 7: 29.
- Robertson, J, Lang, S, Lambert, PA, Martin, PE. Peptidoglycan derived from Staphylococcus epidermidis induces Connexin43 hemichannel activity with consequences on the innate immune response in endothelial cells. Biochem J. 2010; 432(1): 133-43.
- Rosenberg, GA. Neurological diseases in relation to the blood–brain barrier. J. Cereb Blood Flow Metab. 2012; 32: 1139–1151.
- Rothenberg, ML, Oza, AM, Bigelow, RH, Berlin, JD, Marshall, JL, Ramanathan, RK, Hart, LL, Gupta, S, Garay, CA, Burger, BG, Le Bail, N, Haller, DG. Superiority of oxaliplatin and fluorouracil-leucovorin compared with either therapy alone in patients with progressive colorectal cancer after irinotecan and fluorouracil-leucovorin: interim results of a phase III trial. J Clin Oncol. 2003. 21: 2059-2069.
- Roux, F, Couraud, PO. Rat brain endothelial cell lines for the study of blood-brain barrier permeability and transport functions. Cell Mol Neurobiol. 2005; 25(1): 41-58.
- Sá-Pereira et al. Neurovascular unit: a focus on pericytes. Mol Neurobiol. 2012; 4: 327–347.
- Saez, JC, Berthoud, VM, Branes, MC, Martinez, AD, Beyer, EC. Plasma membrane channels formed by connexins: their regulation and functions. Physiol Rev. 2003; 83(4): 1359-400.
- Saif, MW, Reardon, J. Management of oxaliplatin-induced peripheral neuropathy. Ther Clin Risk Manag. 2005; 1(4): 249-58.
- Sanchez, A, Tripathy, D, Luo, J, Yin, X, Martinez, J and Grammas, P. Neurovascular unit and the effects of dosage in VEGF toxicity: role for oxidative stress and thrombin. J Alzheimers Dis. 2013; 34: 281–291.

- Sauer, R, Becker, H, Hohenberger, W, et al. Preoperative versus postoperative chemoradiotherapy for rectal cancer. N Engl J Med. 2004; 351: 1731-40.
- Schock, SC, Leblanc, D, Hakim, AM, Thompson, CS. ATP release by way of connexin 36 hemichannels mediates ischemic tolerance in vitro. Biochem Biophys Res Commun. 2008; 368 (1): 138-144.
- Shepro, D and Morel, NM. Pericyte physiology. FASEB J. 1993; 7: 1031–1038.
- Shiu, C, Barbier, E, Cello, FD, Choi, HJ, and Stins, M. HIV-1 gp120 as well as alcohol affect blood-brain barrier permeability and stress fiber formation: involvement of reactive oxygen species. Alcohol Clin Exp Res. 2007; 31: 130–137.
- Siegel, RL, Miller, KD, Jemal, A. Cancer statistics. CA Cancer J Clin. 2016; 66: 7-30.
- Simard, M, Arcuino, G, Takano, T, Liu, QS, Nedergaard, M. Signaling at the gliovascular interface. J Neurosci. 2003; 23: 9254-62.
- Simpson, IA, Vannucci, SJ, DeJoseph, MR, Hawkins, RA. Glucose transporter asymmetries in the bovine blood-brain barrier. J Biol Chem. 2001; 276: 12725–12729.
- Smith, EM, Pang, H, Ye, C, Cirrincione, C, Fleishman, S, Paskett, ED, Ahles, T, Bressler, LR, Le-Lindqwister, N, Fadul, CE, Loprinzi, C, Shapiro, CL. Alliance for Clinical Trials in Oncology. Predictors of duloxetine response in patients with oxaliplatin-induced painful chemotherapy-induced peripheral neuropathy (CIPN): a secondary analysis of randomised controlled trial - CALGB/alliance 170601. Eur J Cancer Care (Engl). 2015; doi: 10.1111/ecc.12421. [Epub ahead of print].
- Soker, S, Miao, H-Q, Nomi, M, Takashima, S and Klagsbrun, M. VEGF165 mediates formation of complexes containing VEGFR-2 and neuropilin-1 that enhance VEGF165-receptor binding. J Cell Biochem. 2002; 85: 357–368.
- Song, L, Ge, S, and Pachter, JS. Caveolin-1 regulates expression of junction-associated proteins in brain microvascular endothelial cells.

Blood. 2007;109: 1515–1523.

- Sperlagh, B, Vizi, ES, Wirkner, K, Illes, P. P2X7 receptors in the nervous system. Prog Neurobiol. 2006; 78: 327-346.
- Spray, DC, Hanani, M. Gap junctions, pannexins and pain. Neurosci Lett. 2017; S0304-3940 (17) 30515-3.
- Stamatovic, SM, Johnson, AM, Keep, RF, Andjelkovic, AV. Junctional proteins of the blood-brain barrier: New insights into function and dysfunction. Tissue Barriers. 2016; 4(1): e1154641.
- Stanimirovic, DB, and Friedman, A. Pathophysiology of the neurovascular unit disease cause or consequence? J. Cereb.BloodFlowMetab. 2012; 32, 1207–1221.
- Tabbì, G, Magrì, A, Giuffrida, A, Lanza, V, Pappalardo, G, Naletova, I, Nicoletti VG, Attanasio, F, Rizzarelli, E. Semax, an ACTH4-10 peptide analog with high affinity for copper(II) ion and protective ability against metal induced cell toxicity. J Inorg Biochem. 2015; 142: 39-46.
- Thompson, RJ, Zhou, N, MacVicar, BA. Ischemia opens neuronal gap junction hemichannels. Science. 2006; 312: 924-7.
- Thore, S, Dyachok, O, Gylfe, E, Tengholm, A. Feedback activation of phospholipase C via intracellular mobilization and store-operated influx of Ca2+ in insulin-secreting beta-cells. J Cell Sci. 2005; 118(Pt 19): 4463-71.
- Tournigand, C, Andre, T, Achille, E, Lledo, G, Flesh, M, et al. FOLFIRI followed by FOLFOX6 or the reverse sequence in advanced colorectal cancer: a randomized GERCOR study. J Clin Oncol. 2004; 22: 229-37.
- Tsuda, M, Tozaki-Saitoh, H, Inoue, K. Pain and purinergic signaling. Brain Res Rev. 2010; 63: 222-232.
- Vorbrodt, AW, Dobrogowska, DH. Molecular anatomy of intercellular junctions in brain endothelial and epithelial barriers: electron microscopist's view. Brain Res Brain Res Rev. 2003; 42: 221–242.
- Walter, JK, Castro, V, Voss, M, Gast, K, Rueckert, C, Piontek, J, Blasig, IE. Redox sensitivity of the dimerization of occludin. Cell Mol Life Sci 2009; 66: 3655–3662.

- Wang, M, Wey, S, Zhang, Y, Ye, R, Lee, AS. Role of the unfolded protein response regulator GRP78/BiP in development, cancer, and neurological disorders. Antioxid Redox Signal. 2009; 11(9): 2307-16.
- Wang, N, De Bock, M, Decrock, E, Bol, M, Gadicherla, A, Vinken, M, Rogiers, V, Bukauskas, FF, Bultynck, G, Leybaert, L. Paracrine signaling through plasma membrane hemichannels. Biochim Biophys Acta. 2013; 1828(1): 35-50.
- Webster, RG, Brain, KL, Wilson, RH, Grem, JL, Vincent, A. Oxaliplatin induces hyperexcitability at motor and autonomic neuromuscular junctions through effects on voltage-gated sodium channels. Br J Pharmacol. 2005; 146(7): 1027-39.
- Wei, R, Wang, J, Xu, Y, Yin, B, He, F, Du, Y, Peng, G, Luo B. Probenecid protects against cerebral ischemia/reperfusion injury by inhibiting lysosomal and inflammatory damage in rats. Neuroscience. 2015; 301: 168-77.
- Wieseler-Frank, J, Maier, SF, Watkins, LR. Glial activation and pathological pain. Neurochem. Int. 2004; 45: 389-395.
- Winkler, EA, Bell, RD and Zlokovic, BV. Central nervous system pericytes in health and disease. Nat. Neurosci. 2011; 14: 1398-1405.
- Winkler, MKL, Chassidim, Y, Lublinsky, S, Revankar, GS, Major, S, Kang, E-J. Impaired neurovascular coupling to ictal epileptic activity and spreading depolarization in a patient with subarachnoid hemorrhage: possible link to blood-brain barrier dysfunction. Epilepsia. 2012; 53(Suppl 6): 22–30.
- Wolburg, H et al. Brain endothelial cells and the glio-vascular complex. CellTissueRes. 2009; 335, 75–96.
- Wolburg, H. The Endothelial Frontier. In Blood-Brain Interface: From Ontogeny to Artificial Barriers, R. Dermietzel, D.C. Spray, and M. Nedergaard, eds. (Weinheim, Germany: Wiley-VCH) 2006; pp. 77–109.
- Wolf, S, Barton, D, Kottschade, L, Grothey, A, Loprinzi, C. Chemotherapy induced peripheral neuropathy: prevention and treatment strategies Eur J Cancer. 2008; 44: 1507–1515.

- Wong, AD, Ye, M, Levy, AF, Rothstein, JD, Bergles, DE, and Searson, PC. The blood-brain barrier: an engineering perspective. Front. Neuroeng. 2013; 6: 7.
- Wu, KC, Lu, YH, Peng, YH, Tsai, TF, Kao, YH, Yang, HT, Lin, CJ. Decreased expression of organic cation transporters, Oct1 and Oct2, in brain microvessels and its implication to MPTP-induced dopaminergic toxicity in aged mice. J Cereb Blood Flow Metab. 2015; 35(1): 37-47.
- Yang, F, Zhao, K, Zhang, X, Zhang, J, Xu, B. ATP induces disruption of tight junction proteins via IL-1 beta-dependent MMP-9 Activation of human blood–brain barrier in vitro. Neural Plast; 2016: 8928530.
- Yang, Y, Estrada, EY, Thompson, JF, Liu, W, and Rosenberg, GA. Matrix metalloproteinase-mediated disruption of tight junction proteins in cerebral vessels is reversed by synthetic matrix metalloproteinase inhibitor in focal ischemia in rat. J. Cereb. Blood Flow Metab. 2007; 27: 697–709.
- Yen, MR, Saier, MH, Jr. Gap junctional proteins of animals: the innexin/pannexin superfamily. Prog Biophys Mol Biol. 2007; 94: 5-14.
- Zamboni, WC, Gervais, AC, Egorin, MJ, Schellens, JH, Hamburger, DR, Delauter, BJ, Grim, A, Zuhowski, EG, Joseph, E, Pluim, D, Potter, DM, Eiseman, JL. Inter- and intratumoral disposition of platinum in solid tumors after administration of cisplatin. Clin Cancer Res. 2002; 8: 2992–2999.
- Zanardelli, M, Micheli, L, Cinci, L, Failli, P, Ghelardini, C, Di Cesare Mannelli, L. Oxaliplatin neurotoxicity involves peroxisome alterations. PPARγ agonism as preventive pharmacological approach. PLoS One. 2014; 9(7): e102758.
- Zhang, S, Lovejoy, KS, Shima, JE, Lagpacan, LL, Shu, Y, Lapuk, A, Chen, Y, Komori, T, Gray, JW, Chen, X, Lippard, SJ, Giacomini, KM. Organic cation transporters are determinants of oxaliplatin cytotoxicity. Cancer Res. 2006; 66(17): 8847-57.
- Zhang, Y, Laumet, G, Chen, SR, Hittelman, WN, Pan, HL. Pannexin-1 Up-regulation in the Dorsal Root Ganglion Contributes to Neuropathic Pain Development. J Biol Chem. 2015; 290(23): 14647-55.

- Zlokovic, BV. The blood-brain barrier in health and chronic neurodegenerative disorders. Neuron. 2008; 57(2): 178-201.
- Zonta, M, Angulo, MC, Gobbo, S, Rosengarten, B, Hossmann, KA, Pozzan, T et al. Neuron-to-astrocyte signaling is central to the dynamic control of brain microcirculation. Nat Neurosci. 2003; 6: 43–50.

Acknowledgments

I am sincerely grateful to my supervisor Prof. Carla Ghelardini for giving me the opportunity to carry out this PhD research and for her continuous support and precious advice.

Further, I would like to thank Prof. Luc Leybaert for giving me the possibility to do research in his lab allowing me to enrich my PhD project with this experience.

I wish even to thank very much Dr. Lorenzo Di Cesare Mannelli for conveying to me his knowledge and his enthusiasm in pharmacology, and for helping me in developing critical thinking. I would like to thank Dr. Alessandra Pacini for her precious help in the development of this PhD project and for the pricelss advices in the anatomic field.

I would finally thank all my collagues and my family.